



Sofia University "St. Kliment Ohridski"  
Faculty of Mathematics and Informatics  
Department of Numerical Methods and  
Algorithms

## Numerical simulations of the process of adsorption onto activated carbon in water treatment applications

MASTER'S THESIS  
IN COMPUTATIONAL MATHEMATICS AND MATHEMATICAL MODELLING

**Author:** Maria N. Zarcheva, FN 25940  
**Supervisor:** Assist. Prof. Dr. Tihomir B. Ivanov

March, 2020

## Abstract

Mathematical modelling and computer simulations are a powerful tool for the exploitation and management of water resources—an important current topic in environmental and engineering science. The Master’s thesis is concerned with modelling water treatment using adsorption onto activated carbon filters—a widely used technology, whose proper management is essential for its effectiveness.

A relatively simple mathematical model has been recently developed by a Dutch water cycle research institute. It was presented at a European Study Group with Industry in the beginning of 2019. It comprises of  $2N$  non-linear advection–adsorption partial differential equations, where  $N$  is the number of contaminants in the water. The numerical solution of this model, however, was identified as a current problem for various values of the model parameters.

The main goal of the Master’s thesis is the construction of a robust and efficient numerical scheme for solving the model. To this end, we derive and compare two finite difference schemes. One of them meets the requirements of robustness and efficiency, as validated for a wide range of model parameters, expected to be encountered in practice. This scheme is used in the thesis to carry out various numerical experiments that aim to simulate qualitatively the process of adsorption of natural organic matter and different micro-pollutants onto activated carbon. It is successfully applied to the solution of the system of 20 PDEs, corresponding to 10 contaminants in the water.

One of the main reasons for simulating the process is the prediction of the time when a particular carbon filter will get exhausted and needs to be replaced. Thus, we compute so-called breakthrough curves that give information about the quality of the water treatment (i.e., how much of the pollutant is still present in the water after passing through the filter). This also allows us to make a comparison between the adsorption properties of the 10 considered contaminants.

Further, in order to improve the computational efficiency of the numerical scheme, we suggest an approximation of the non-linear term using spline interpolation. The approach is derived for the cases of one and two contaminants. Linear and bilinear splines are used, respectively. Numerical experiments illustrate the applicability of this approach.

# Contents

<b>1</b>	<b>Introduction</b>	<b>5</b>
1.1	Fundamentals of adsorption onto activated carbon in water and wastewater treatment . . . . .	5
1.1.1	Adsorption . . . . .	6
1.2	Adsorption equilibrium and isotherms . . . . .	10
1.2.1	Single-solute adsorption and the Freundlich isotherm . . . . .	11
1.2.2	Multi-solute adsorption . . . . .	12
1.3	Mathematical modelling . . . . .	13
1.3.1	Mathematical model . . . . .	13
1.3.2	Nondimensionalization . . . . .	15
1.4	Goals and structure of the Master's thesis . . . . .	15
<b>2</b>	<b>Numerical schemes</b>	<b>17</b>
2.1	Semi-implicit scheme . . . . .	17
2.2	Fully-implicit Scheme . . . . .	18
2.3	Practical aspects of implementing the schemes . . . . .	19
<b>3</b>	<b>Numerical experiments</b>	<b>21</b>
3.1	Qualitative results for the process of adsorption . . . . .	23
3.1.1	Single-solute modelling . . . . .	23
3.1.2	Multi-solute adsorption modelling . . . . .	28
3.2	Breakthrough curves . . . . .	36
3.3	Regarding the reverse process: desorption . . . . .	42
3.4	Performance of the numerical schemes . . . . .	43
3.4.1	Using a semi-implicit scheme and the influence of $\gamma$ . . . . .	43
3.4.2	Practical estimate of order of convergence . . . . .	45
3.4.3	Computational times . . . . .	46
<b>4</b>	<b>Approximation of the adsorption capacity</b>	<b>47</b>
4.1	Univariate spline interpolation in the one-contaminant case . . . . .	47
4.2	Bivariate spline interpolation in the two-contaminant case . . . . .	55
	<b>Conclusion and perspectives</b>	<b>62</b>

<b>A Breakthrough curves</b>	<b>67</b>
<b>B Management of spent material</b>	<b>69</b>
<b>C Spline interpolation basics</b>	<b>71</b>
C.1 Univariate spline interpolation . . . . .	71
C.2 Bivariate spline interpolation . . . . .	73

## Nomenclature

$N$	number of contaminants
$Q_i$	adsorption capacity (load function) of $i$ -th contaminant ( $MM^{-1}$ )
$c_{e_i}$	equilibrium concentration of $i$ -th contaminant ( $ML^{-3}$ )
$1/n_i$	Freundlich isotherm intensity parameter for $i$ -th contaminant (-)
$K_{F_i}$	Freundlich adsorption constant of $i$ -th contaminant ( $MM^{-1}(L^3 M^{-1})^{1/n_i}$ )
$n'$	average value of $n_i, i = 1, \dots, N$
$K_{F'}$	average value of $K_{F_i}, i = 1, \dots, N$
$c_0 (c_{i,0})$	input liquid-phase concentration (for contaminant $i$ ) ( $ML^{-3}$ )
$c_i$	liquid-phase concentration for contaminant $i$ ( $ML^{-3}$ )
$c_{ch}$	characteristic liquid-phase concentration ( $ML^{-3}$ )
$q_i$	solid phase concentration (load) for contaminant $i$ ( $MM^{-1}$ )
$\nu$	velocity of the water flow ( $LT^{-1}$ )
$\epsilon$	porosity of the filter bed (-)
$\gamma$	rate of transfer of compound from the outer surface of AC to its interior ( $T^{-1}$ )
$D_s$	intraparticle diffusion coefficient ( $L^2 T^{-1}$ )
$d_p$	AC particle diameter ( $L$ )
$\rho$	density of carbon ( $ML^{-3}$ )
$MW_i$	molar weight of contaminant $i$ (-)
$Q_{I,h_s}$	linear/bilinear spline interpolant of the load function

## List of Abbreviations

AC	Activated Carbon
IAST	Ideal Adsorbed Solution Theory
SIAS	Simplified Ideal Adsorbed Solution
ISIAS	Improved Simplified Ideal Adsorbed Solution
GAC	Granular Activated Carbon
PAC	Powdered Activated Carbon
MTZ	Mass Transfer Zone
NOM	Natural Organic Matter

# Chapter 1

## Introduction

### 1.1 Fundamentals of adsorption onto activated carbon in water and wastewater treatment

Activated carbon (see Figure 1.1) is highly porous medium, capable of removing large variety of pollutants from water and wastewater through the process of adsorption. It usually comes in one of the following forms—granular activated carbon (GAC) and powdered activated carbon (PAC). This material is suitable because of its large internal surface area ( $500\text{--}1500\text{ }m^2g^{-1}$ ), while the pore volume ranges between 0.7 and  $1.8\text{ }cm^3g^{-1}$  [3].

Since adsorption is the main process that allows the water treatment by carbon filters (see Figure 1.2), we shall first discuss it in some detail.



(a) Powdered activated carbon (PAC)      (b) Granular activated carbon (GAC)

Figure 1.1: Types of activated carbon.

### 1.1.1 Adsorption

Adsorption is an important physical phenomenon that takes place in large variety of processes. **Adsorption is the accumulation of substances (adhesion of particles) on a surface or an interface layer between two phases [3].** The adsorbing phase is called the adsorbent, and the substance, being adsorbed—adsorbate (Figure 1.3). Adsorption can occur between two phases, namely, liquid-liquid, gas-liquid, gas-solid, or liquid-solid interfaces. In the case of activated carbon water purification, the adsorbent is a solid phase. As a result of the process, the adsorbate forms a thin film on the surface of the adsorbent. **Let us reemphasize that the phenomenon of increased concentration of the soluble material on a boundary or surface is commonly referred to as adsorption.**



Figure 1.2: Carbon columns [9].

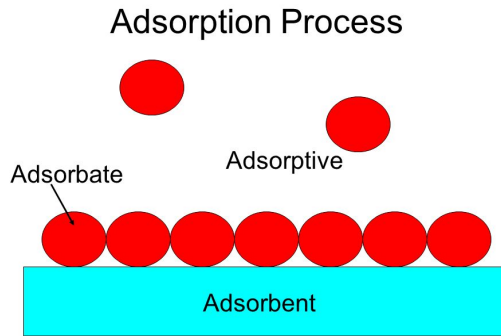


Figure 1.3: Adsorption process. Adsorbate and adsorbent [20].

This phenomenon occurs due to surface energy. A particle that comes in contact with the surface does not have enough energy to leave it. There could be two main reasons for this:

**Physical adsorption.** Physical adsorption (physisorption) occurs because of van der Waals forces. Exchange of electrons between the phases does not occur in physisorption, meaning that the adsorbed particles continue their free thermal motion within the surface of the adsorbent (Figure 1.4). If the speed of a particular molecule is large enough, it can detach from the surface and return back to the solute. **The latter process is known as desorption.**

**Chemical adsorption.** In chemical adsorption, also termed as chemisorption, a chemical reaction occurs between the adsorbate and the adsorbent. Unlike physisorption, the adsorbed particles are not free to move within the surface, nor to leave it anymore. This is because, during the chemical reaction, chemical bonds between adsorbate and adsorbent particles are established (Figure 1.4).

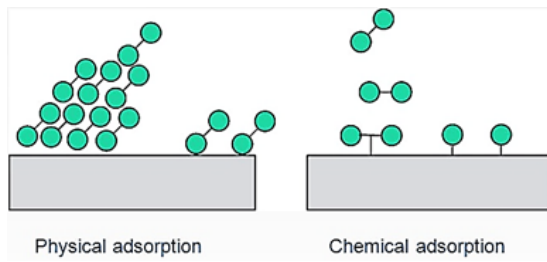


Figure 1.4: Physisorption and chemisorption [22].

It is very difficult to distinguish between these two kinds of adsorption. Often, both of them can be observed in the same system. Usually, the chemisorption is preceded by physisorption.

We should also note that for the intensity of adsorption a very important factor is the solubility of the adsorbate. Hydrophilic substances are less adsorbable than hydrophobic ones. Some complex organic compounds that have both hydrophilic and hydrophobic groups could be partly adsorbed, i.e., their hydrophobic groups are being adsorbed, whereas their hydrophilic ones are not.

Because of its high porosity, activated carbon has large surface area. Therefore, it is particularly appropriate for water treatment applications, based on adsorption. The process can be characterized with the following steps (Figure 1.5) [3]:

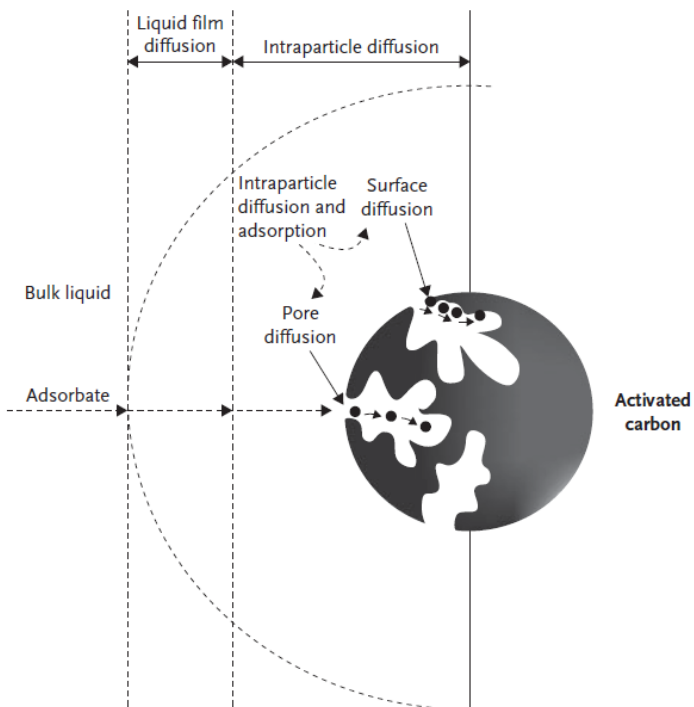


Figure 1.5: External and internal transport of an adsorbate in an activated carbon particle [3].

1. **Bulk solution transport** from the ambient solution (bulk liquid) to the vicinity of the adsorbent particle. Activated carbon particles are consid-

ered to be surrounded by a liquid film (boundary layer of water). Adsorbates must first be transported from the bulk (ambient) solution into this layer. This process may occur through diffusion or turbulent mixing (random transport of particles).

2. **External diffusion (liquid-phase diffusion).** The molecules of the solute need to be transferred through the liquid film, surrounding the carbon particles, to their surface. Mass transport through this layer occurs by diffusion, resulting from concentration difference.
3. **Internal diffusion (solid-phase diffusion).** The transfer of adsorbate from the surface of a carbon particle to sites within the particle is termed internal (intraparticle) diffusion. The rate of this process is determined primarily by the pore structure of the particle. There are two types of intraparticle diffusion—pore diffusion and surface diffusion (see Figure 1.5). Pore diffusion refers to the natural thermal motion of the solutes within the fluid-filled pores. Surface diffusion is the free movement of adsorbate molecules over the internal surface of the adsorbent. This phenomenon only occurs when molecules are already adsorbed and provided the surface attractive forces are not strong enough to prevent mobility of the adsorbed species. The molecules then are free to move over the surface to other vacant adsorption sites. Surface diffusion is more significant in adsorbents with large surface area and narrow pores. Often, pore diffusion and surface diffusion are termed macropore and micropore diffusion, respectively. These two modes of intraparticle diffusion usually act in parallel. In water treatment process modelling, the surface diffusion is usually assumed to be the dominant intraparticle transport mechanism [3].
4. **Adsorption.** When an adsorbate particle has reached an available site, an adsorption bond is formed.

**The slowest step among the preceding four, called rate-limiting step, controls the overall rate of the removal of contaminant from the solution.** Physical adsorption is considered to happen very rapidly (therefore, in the case of physical adsorption, one of the diffusion steps will be the rate-limiting one), whereas chemisorption can be significantly slower and, thereby, control the total rate of removal [3].

The main factors that influence adsorption are:

- Surface area of the adsorbent  
The specific surface area refers to the part of the total surface area of the adsorbent that is capable to adsorb. The finer the porosity of the adsorbent, the more intensive the adsorption.
- Porosity of the adsorbent  
For the quality of the adsorbent, a very important feature is its internal

structure, i.e., the size and distribution of its pores. Usually, the pores are classified in three groups, depending on their size—micropores (width not exceeding 2 nm), mesopores (width between 2 and 50 nm) and macropores (width greater than 50 nm) [3]. The size of the pores determines the accessibility of adsorbate molecules to the internal adsorption surface. The greatest part of the total specific surface area is found in the micropores. Their sizes are comparable to those of adsorbate molecules. In some sense, the actual adsorption takes place exactly in the micropores, whereas macro- and mesopores serve as a path for the adsorbate molecules to reach the interior of the particle.

- Chemical characteristics of the adsorbate

The capability of a substance to be adsorbed is tightly related to its chemical properties. As pointed earlier, the solubility of the solute is of great importance for the process. If the solute is highly soluble, then the solute–solvent bonds are stronger than the attractive forces between the solute and the adsorbent. Other properties of the adsorbate, which are of primary concern for adsorption, are the size of its molecules, their polarity, dissociation constants, etc.

- pH

Adsorption of most organic materials is higher at neutral conditions.

- Temperature

Although adsorption is an exothermic process, its rate is increased at a higher temperature, because increased temperature also increases the rate of diffusion of the solute through the liquid to the adsorption sites, which eventually leads to an increased adsorption [3].

## 1.2 Adsorption equilibrium and isotherms

Adsorption is usually studied in stirred batch reactors, i.e., where the pollutant concentration is uniform and there are no feed or exit streams. As we said, the reverse process of adsorption is termed desorption and it is the phenomenon of releasing an adsorbed substance from or through a surface.

The molecules that manage to detach from the surface are those, which have sufficient thermal energy to break the bond with a specific site on the surface, while vibrating about it. With temperature rising, the amount of particles having enough energy to break the attachment bond rises [9].

When the rate of the forward reaction (adsorption) equals the rate of the reverse reaction (desorption), an equilibrium is reached and no further accumulation on the surface of the carbon particles occurs. At this state, a defined distribution of the adsorbed material among the adsorbent phase and the solution phase exists.

This distribution is represented by the so-called **adsorption isotherm**. The

adsorption isotherm at temperature  $T$  is the relation

$$Q = Q(c_e) \text{ at temperature } T,$$

where  $c_e$  is the equilibrium concentration of the adsorbate in the liquid phase and  $Q$  is the adsorbed amount of contaminant per unit weight of adsorbent at the fixed temperature  $T$ .

The amount adsorbed per unit weight of the adsorbent increases with increasing equilibrium concentration but not in direct proportion. Most favourable shape of an isotherm curve is convex upward, as shown in Figure 1.6 [3]. This isotherm is the primary source of information about the process and is very useful in estimating its quality. The two most popular isotherm curve models, both of them empirical, are the so-called Freundlich isotherm and Langmuir isotherm. The latter will not be discussed in the Master's thesis. More information about it can be found, e.g., in [3].

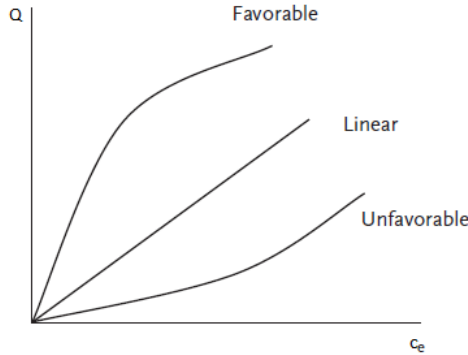


Figure 1.6: Types of isotherm curves [3].

### 1.2.1 Single-solute adsorption and the Freundlich isotherm

**Freundlich isotherm** [7] is applicable to adsorbents that are assumed to have heterogeneous surface, consisting of sites with different adsorption potentials. This relationship is entirely empirical and is very widely used for activated carbon applications. It can be expressed as

$$Q = K_F c_e^{1/n}, \quad (1.1)$$

where  $Q$  is the adsorption capacity (mg adsorbate, adsorbed per g adsorbent),  $c_e$  is the equilibrium adsorbate concentration,  $K_F$  is called Freundlich adsorption constant and  $1/n$ —Freundlich slope. All experiments in the present work are based on this isotherm and its generalization, outlined in the next subsection.

$K_F$  and  $1/n$  are empirical constants that represent adsorption capacity and adsorption intensity (slope of the isotherm curve), respectively, and characterize the specific adsorbate.

### 1.2.2 Multi-solute adsorption

The adsorption theories, mentioned above, are based on single-solute adsorption, i.e., when there is a single adsorptive substance, present in the solution. However, in water treatment applications, the most common case is the presence of multiple solutes in the water that compete with each other for adsorption sites. Therefore, we outline some multi-solute adsorption theories below.

Usually, multi-solute adsorption is characterized by the same parameters as the single-solute one. This means that multi-solute adsorption theories can be directly derived from the Freundlich or Langmuir isotherms. However, as mentioned above, the competition between the adsorbates must be accounted for. Several theoretical approaches exist for predicting multi-component equilibria. The most popular theory concerning adsorption equilibria is the Ideal Adsorbed Solution Theory (IAST). Its name comes from the assumption that the adsorbed materials form an “ideal solution”. In fact, two simplifications of this theory are commonly used in adsorption modelling: The Simplified Ideal Adsorbed Solution (SIAS) model, and the Improved Simplified Ideal Adsorbed Solution (ISIAS) model. We shall use those in the Master’s thesis and, thus, outline them below. The general theory is described, e.g., in [1, 11].

Let there be  $N$  substances,  $i = 1, \dots, N$ . According to the **SIAS** model [5], each individual loading in the mixture can be calculated using the following relation:

$$Q_i = K_{F'}^{\left(\frac{n'-1}{n'}\right)} \left[ K_{F_i} c_{e_i}^{n_i} \right]^{1/n'} \left[ \sum_{i=1}^N \left( \frac{K_{F_i}}{K_{F'}} c_{e_i}^{n_i} \right)^{1/n'} \right]^{(n'-1)}, \quad (1.2)$$

where  $Q_i$  is the solid phase equilibrium concentration (adsorption capacity) of solute  $i$ ,  $K_{F_i}$  and  $n_i$  are the corresponding single-solute empirical Freundlich constants for solute  $i$ ,  $c_{e_i}$  is the liquid phase equilibrium concentration of solute  $i$ ,  $n'$  and  $K_{F'}$  are the average values of  $n_i$  and  $K_{F_i}$ ,  $i = 1, \dots, N$ , respectively.

**ISIAS** model [14] was developed as a modification of SIAS to account for the competition for adsorption sites by adding a competition factor denoted below as ‘ $a$ ’:

$$Q_i = K_{F'}^{\left(\frac{n'-1}{n'}\right)} \left[ \frac{K_{F_i}}{a_i} c_{e_i}^{n_i} \right]^{1/n'} \left[ \sum_{i=1}^N \left( \frac{K_{F_i}/a_i}{K_{F'}} c_{e_i}^{n_i} \right)^{1/n'} \right]^{(n'-1)}, \quad (1.3)$$

where

$$K_{F'} = \frac{\sum(K_{F_i} a_i)}{N}.$$

Let us note that the competition factors need to be estimated from experimental data. For the time being, we assume that all of them are equal to 1, thus, (1.3) reduces to (1.2). I.e., further in the Master's thesis, we only refer to the SIAS model.

## 1.3 Mathematical modelling

### 1.3.1 Mathematical model

We shall consider here a simplified 1D model of the process of water purification with carbon filters, being developed by KWR Watercycle Research Institute [12, 28]. Let there be  $N$  different contaminants in the water. Each contaminant is characterized by two main quantities:

- $c_i, i = 1, \dots, N$ —the concentration of the  $i$ -th contaminant in the liquid phase;
- $q_i, i = 1, \dots, N$ —the amount of the  $i$ -th contaminant inside the carbon particles, often termed as “load”.

Let  $t \in [0, T]$  and  $x \in [0, X]$  be the time and spatial variables, respectively, where  $x = X$  corresponds to the inlet of the carbon filter (Figure 1.7). If one assumes that the adsorption (i.e., steps 3 and 4 of the process, described on p. 8) is the rate-limiting process, diffusion is negligible with respect to advection and the water flow rate inside the column is constant, the following advection–adsorption model can be formulated:

$$\begin{aligned} \frac{\partial c_i}{\partial t} &= \frac{\nu}{\epsilon} \frac{\partial c_i}{\partial x} - \rho \frac{1-\epsilon}{\epsilon} \gamma (Q_i - q_i), \\ \frac{\partial q_i}{\partial t} &= \gamma (Q_i - q_i). \end{aligned} \quad (1.4)$$

We close the system with the following initial and boundary conditions:

$$c_i(x, 0) = 0, \quad q_i(x, 0) = 0, \quad c_i(X, t) = c_{0,i}. \quad (1.5)$$

The physical meaning of the given quantities is as follows:

- $\nu$  is the constant velocity of the water flow;
- $\epsilon$  is the porosity of the filter bed (the fraction of voids volume over the total body volume);
- $\gamma = \frac{6 \cdot 10 \cdot D_s}{d_p^2}$  is the rate of transfer of a compound from the outer surface of the particle to its interior, where  $D_s$  is the intraparticle diffusion coefficient and  $d_p$  is the activated carbon particle diameter;
- $\rho$  is the density of carbon;

- $Q_i$  is the load of compound  $i$  on the surface of the carbon particle (the solid phase concentration at the outer surface of the AC particle). We further model it in two possible ways:

– using simply the Freundlich isotherm (for  $N = 1$ )

$$Q_i = K_{F,i} c_i^{1/n_i}; \quad (1.6)$$

– using SIAS model (1.2).

We shall often refer to the function  $Q_i$  as the **load function** of the  $i$ -th contaminant.

One important remark to make here is that IAST is valid for molar liquid and solid phase (IAST is defined for molar mass of the contaminants). Since, usually, the Freundlich constant is given in the literature in  $(\text{mol}/\text{kg})/(\text{mol}/\text{m}^3)^{n_i}$  (let us denote this value by  $\bar{K}_{F,i}$ ), one needs to make the following change to  $(\text{g/g})/(\text{g}/\text{m}^3)^{n_i}$  [1]:

$$K_{F,i} = 1000 M W_i^{(n_i-1)} \bar{K}_{F,i},$$

where  $M W_i$  is the molar weight of component  $i$  ( $\text{g/mol}$ ).

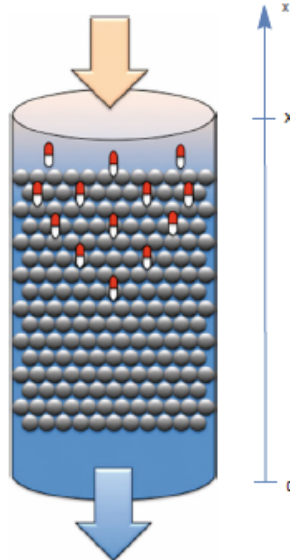


Figure 1.7: Inlet and outlet of a GAC filter.

### 1.3.2 Nondimensionalization

We introduce the following nondimensionalization of model (1.4), (1.5):

$$\bar{t} = \gamma t, \quad \bar{x} = \frac{\gamma}{\nu} x, \quad \bar{c}_i = \frac{c_i}{c_{ch}}, \quad \bar{q}_i = \frac{\rho q_i}{c_{ch}}, \quad (1.7)$$

where  $c_{ch}$  is some characteristic concentration that we shall specify later. Skipping the bars for notational simplicity, we obtain

$$\begin{aligned} \frac{\partial c_i}{\partial t} &= \frac{1}{\epsilon} \frac{\partial c_i}{\partial x} - \frac{1-\epsilon}{\epsilon} (Q_i - q_i), \\ \frac{\partial q_i}{\partial t} &= Q_i - q_i, \end{aligned} \quad (1.8)$$

$i = 1, \dots, N$ , where  $Q_i$  can be modelled in one of the following ways after the change of variables:

- Freundlich isotherm

$$Q_i = \frac{\rho}{c_{ch}} K_{F,i} (c_{ch} c_i)^{\frac{1}{n_i}}, \quad (1.9)$$

- SIAS model

$$Q_i = \frac{\rho}{c_{ch}} K_F^{\left(\frac{n'-1}{n'}\right)} [K_{F,i} (c_i c_{ch})^{n_i}]^{1/n'} \left[ \sum_{i=1}^N \left( \frac{K_{F,i}}{K_{F'}} (c_i c_{ch})^{n_i} \right)^{1/n'} \right]^{(n'-1)}. \quad (1.10)$$

The initial and boundary conditions become

$$c_i(x, 0) = 0, \quad q_i(x, 0) = 0, \quad c_i(X, t) = \frac{c_0}{c_{ch}}. \quad (1.11)$$

## 1.4 Goals and structure of the Master's thesis

In order to validate and use the mathematical model for simulating water treatment with AC filters, one needs robust and efficient numerical schemes. In [12], it was pointed as a problem that the numerical methods, used by KWR institute [28] have serious convergence problems for various values of the model parameters, corresponding to micro-pollutants. During SWI 2019 (Dutch European Study Group with Industry), some ideas were proposed towards solving the differential problem in the case of one contaminant.

The goals of the Master's thesis are as follows:

- To propose a robust numerical method for simulating multi-component adsorption, based on the model (1.8), (1.10), (1.11);
- To study qualitatively the processes of adsorption and desorption based on numerical experiments;

- To simulate the adsorption process for various pollutants and to make comparison between their adsorption properties;
- To show how results about the exhaustion of a particular carbon filter can be obtained, using the proposed methods, by computing so-called breakthrough curves;
- To propose appropriate approximations of the function (1.10), which allow its more efficient computation, seeking to improve the performance of the numerical schemes;
- To outline possible directions for future development of the study.

The Master's thesis is structured as follows. In Chapter 2, two finite difference schemes are derived. Numerical experiments, based on their implementation are provided in Chapter 3. In particular, the adsorption process is successfully simulated for ten different contaminants, present in the water. A discussion is made on the effect of the competition between the contaminants. The effectiveness of water treatment is simulated by computing the so-called breakthrough curves. Also, some technical questions concerning the application of the numerical schemes are discussed. In Chapter 4, spline approximation of the load function is used in the cases of one and two contaminants. Numerical experiments illustrate the applicability of this approach. In the appendix, some basic statements concerning spline interpolation theory are provided. Some important practical aspects of the process of water treatment with activated carbon are outlined in the appendix, as well.

# Chapter 2

## Numerical schemes

We introduce a uniform mesh in the computational domain, as follows

$$\omega_{h\tau} := \{(x_k, t_j) : x_k = kh, t_j = j\tau, k = 0, \dots, n, j = 0, \dots, m, n = X/h, m = T/\tau\}.$$

Let us denote the approximate solution for the concentrations  $c_i$  and the loads on carbon  $q_i$  of each contaminant  $i = 1, \dots, N$  as follows

$$C_{i,k}^j \approx c_i(x_k, t_j), \quad L_{i,k}^j \approx q_i(x_k, t_j), \quad k = 0, \dots, n, \quad j = 0, \dots, m.$$

Below, we construct two finite difference schemes, approximating (1.8), (1.11), both of them with local approximation error  $O(h + \tau)$ . For the spatial derivative, in the first equation of (1.8), we use forward difference formula, taking into account the sign of the advection coefficient [6].

### 2.1 Semi-implicit scheme

First, we construct a semi-implicit scheme by approximating implicitly only the adsorption term in the first equation of (1.8). For  $i = 1, \dots, N$ :

$$\begin{aligned} \frac{C_{i,k}^{j+1} - C_{i,k}^j}{\tau} &= \frac{1}{\epsilon} \frac{C_{i,k+1}^j - C_{i,k}^j}{h} - \frac{1-\epsilon}{\epsilon} (Q_i(C_{1,k}^{j+1}, \dots, C_{N,k}^{j+1}) - L_{i,k}^{j+1}), \\ &\quad k = 0, \dots, n-1, \quad j = 0, \dots, m-1, \\ \frac{L_{i,k}^{j+1} - L_{i,k}^j}{\tau} &= Q_i(C_{1,k}^j, \dots, C_{N,k}^j) - L_{i,k}^j, \quad k = 0, \dots, n, \quad j = 0, \dots, m-1, \\ C_{i,k}^0 &= 0, \quad L_{i,k}^0 = 0, \quad k = 0, \dots, n, \\ C_{i,n}^j &= \frac{c_0}{c_{ch}}, \quad j = 0, \dots, m. \end{aligned} \tag{2.1}$$

This accomplishes two things. First, as suggested in [12], the main limitations on the time step in the corresponding explicit scheme are associated with the

non-linear adsorption term. Thus, we aim to relax the requirements on  $\tau$ . And second, in the multi-component case, this approach will lead to the necessity of solving a system of  $N$  non-linear algebraic equations at each point  $x_k$ , where  $N$  is the number of contaminants. This is much simpler than solving the full system, derived in the next section. The semi-implicit scheme results in the following algorithm:

For  $j = 0, \dots, m - 1$  :

- Compute  $L_{i,k}^{j+1} = (1 - \tau)L_{i,k}^j + \tau Q_i(C_{1,k}^j, \dots, C_{N,k}^j)$ ,  $k = 0, \dots, n$ ,  $i = 1, \dots, N$ ;
- For  $k = 0, \dots, n - 1$ , solve the non-linear algebraic system

$$\mathbf{F}_k(C_{1,k}^{j+1}, \dots, C_{N,k}^{j+1}) = \mathbf{0},$$

where  $\mathbf{F}_k = (f_{k,1}, \dots, f_{k,N})^T$  and

$$f_{k,i} = \frac{C_{i,k}^{j+1} - C_{i,k}^j}{\tau} - \left( \frac{1}{\epsilon} \frac{C_{i,k+1}^j - C_{i,k}^j}{h} - \frac{1 - \epsilon}{\epsilon} (Q_i(C_{1,k}^{j+1}, \dots, C_{N,k}^{j+1}) - L_{i,k}^{j+1}) \right);$$

- $C_{i,n}^{j+1} = \frac{c_0}{c_{ch}}$ ,  $i = 1, \dots, N$ .

## 2.2 Fully-implicit Scheme

The scheme, presented in the previous section, was discussed in [12] for the single-contaminant case. Our numerical experiments, as discussed in more detail in the next chapter, show that for very small (but physically sensible!) values of  $\gamma$ , there still exists a severe limitation on  $\tau$ . Thus, the semi-implicit scheme is applicable only within a certain range of  $\gamma$ , as we shall further clarify in Section 3.4. Therefore, we construct here another scheme by approximating the right-hand side of the first equation in (1.8) on the  $j + 1$ -st time layer. Strictly speaking, the thus-obtained scheme is also semi-implicit, because the second equation is approximated explicitly. Nevertheless, we shall refer to it as “the fully-implicit scheme” to distinguish between the two schemes more easily in the text. The approximation is given below:

$$\begin{aligned} \frac{C_{i,k}^{j+1} - C_{i,k}^j}{\tau} &= \frac{1}{\epsilon} \frac{C_{i,k+1}^{j+1} - C_{i,k}^{j+1}}{h} - \frac{1 - \epsilon}{\epsilon} (Q_i(C_{1,k}^{j+1}, \dots, C_{N,k}^{j+1}) - L_{i,k}^{j+1}), \\ k &= 0, \dots, n - 1, \quad j = 0, \dots, m - 1, \\ \frac{L_{i,k}^{j+1} - L_{i,k}^j}{\tau} &= Q_i(C_{1,k}^j, \dots, C_{N,k}^j) - L_{i,k}^j, \quad k = 0, \dots, n, \quad j = 0, \dots, m - 1, \\ C_{i,k}^0 &= 0, \quad L_{i,k}^0 = 0, \quad k = 0, \dots, n, \\ C_{i,n}^j &= \frac{c_0}{c_{ch}}, \quad j = 0, \dots, m, \quad i = 1, \dots, N. \end{aligned} \tag{2.2}$$

In this case, on each time layer, a non-linear algebraic system with  $N(n+1)$  equations needs to be solved. The fully-implicit scheme results in the following algorithm:

For  $j = 0, \dots, m-1$  :

- Compute  $L_{i,k}^{j+1} = (1 - \tau)L_{i,k}^j + \tau Q_i(C_{1,k}^j, \dots, C_{N,k}^j)$ ,  $k = 0, \dots, n$ ,  $i = 1, \dots, N$ ;
- Solve the non-linear algebraic system

$$\mathbf{F}(C_{1,0}^{j+1}, \dots, C_{1,n}^{j+1}, \dots, C_{N,0}^{j+1}, \dots, C_{N,n}^{j+1}) = \mathbf{0},$$

where  $\mathbf{F} = (f_{1,0}, \dots, f_{1,n}, \dots, f_{N,0}, \dots, f_{N,n})^T$  and

$$f_{i,n} = C_{i,n}^{j+1} - \frac{c_0}{c_{ch}}, \quad i = 1, \dots, N,$$

$$f_{i,k} = \frac{C_{i,k}^{j+1} - C_{i,k}^j}{\tau} - \left( \frac{1}{\epsilon} \frac{C_{i,k+1}^{j+1} - C_{i,k}^{j+1}}{h} - \frac{1-\epsilon}{\epsilon} (Q_i(C_{1,k}^{j+1}, \dots, C_{N,k}^{j+1}) - L_{i,k}^{j+1}) \right),$$

$$k = 0, \dots, n-1, \quad i = 1, \dots, N.$$

## 2.3 Practical aspects of implementing the schemes

When one uses the above constructed numerical schemes, some practical questions arise. We discuss them in this section.

- The first challenge that appears in solving the model equations arises from the definition of the load function  $Q_i, i = 1, \dots, N$  itself. For this reason, we need to find a more computationally-effective way of evaluating the functions  $Q_i$ . The most natural thing to do is making preliminary calculations of the involved parameters and store their values, which can be used in further numerical simulations (e.g., the value of the multiplier  $\frac{\rho}{c_{ch}} K_F^{(\frac{n'-1}{n'})}$  (see (1.10)) can be calculated just once, without needing to know the specific value of the argument that is passed to the function). Nevertheless, the resulting preliminary computed functions are still relatively complex. Their further simplification is a separate problem of interest in this work. Some possible suggestions on the solution of this problem are proposed in Chapter 4.
- Because of the definition of  $Q$  (1.10), some round-off errors can lead to very small (in absolute value) negative concentrations, which in turn result in complex values of  $Q$ . Thus, the following is used in the implementation:
  - If a complex number appears, we take only its real part, neglecting the small imaginary part, obtained due to round-off errors;

- Physically sensible values of the solution cannot be negative. Therefore, if a small negative value appears in the solution, we consider it equal to zero.
- The nonlinear algebraic systems need to be solved with an appropriate iteration method. Further in the thesis, all numerical experiments are carried out using the built-in function `FindRoot` in Wolfram Mathematica 11, which implements a version of the Newton-Raphson method [2].

Let us further note that the behaviour of the schemes in terms of numerical stability and convergence is discussed on the basis of numerical experiments in the next chapter.

# Chapter 3

# Numerical experiments

In this chapter, we shall present the results from implementing the derived numerical schemes for solving the mathematical model. In Section 3.1, we explore the qualitative behaviour of the results, obtained with the fully-implicit scheme. First, we show the effectiveness of the scheme for simulating a process of single-solute adsorption. However, as we discussed earlier, in water purification process there is usually more than one contaminant in the water. Thus, we study the process of multi-solute adsorption and compare the adsorptive properties of 10 contaminants. Numerical experiments, related to some important specifics of the process, namely, the breakthrough curves, and the phenomenon of desorption, are discussed in Section 3.2 and Section 3.3, respectively. Finally, in Section 3.4, some technical questions concerning the applicability of both numerical schemes are discussed.

The following parameters are used for all numerical experiments in the present section [12, 25]:

- **Spatial numerical domain** in nondimensional units:  $x \in [0, \gamma/\nu]$ . The rightmost edge (i.e,  $x = \gamma/\nu$ ) corresponds to the top of the filter (the inlet) and  $x = 0$  corresponds to the bottom (the outlet). In physical domain this corresponds to a 1m high filter. The space-discretization step in all experiments is chosen to be  $h = (\gamma/\nu)/10$ .
- **Time numerical domain** in nondimensional units:  $t \in [0, 6]$ . This time interval corresponds to a simulation of about two years in the physical domain. Time discretization step  $\tau = 0.01$ , which corresponds to 1.15741 days.
- **Initial concentrations** for NOM and all micro-pollutants are considered to be  $c_{0,NOM} = 0.054 \text{ g/m}^3$  and  $c_{0,m} = 10^{-3} \text{ g/m}^3$ , respectively.
- **Characteristic concentration**  $c_{ch} = c_{0,NOM} = 0.054$ .
- **Carbon filter characteristics:**

- Porosity  $\epsilon = 0.4$ ;
- Carbon density  $\rho = 440000 \text{ g/m}^3$ ;
- Water flow velocity  $\nu = 0.144 \text{ m/s}$ ;
- In the examination of the qualitative behaviour of the process, a value of  $\gamma = 10^{-7}$  was used. This is physically sensible value [25], regarding the fact that  $10^{-15} < D_s < 10^{-13} [\text{m}^2/\text{s}]$  and  $5.10^{-4} < d_p < 5.10^{-3} [\text{m}]$ .

Numerical experiments were conducted for the contaminants, summarized in Table 3.1.

Number	Contaminant	$K_F$	$n$	MW	$c_0$
1	NOM	0.018	0.9	300.	0.054
2	Furosemide	0.0574	0.34608	330.74	$10^{-3}$
3	Diclofenac	0.0448685006	0.312	296.148	$10^{-3}$
4	Cortisol	0.06435259022	0.3097	362.46	$10^{-3}$
5	Ketoprofen	0.1132444832	0.39543	254.281	$10^{-3}$
6	Phenazone	0.1869332648	0.4237	188.226	$10^{-3}$
7	Pentoxifylline	0.029992813156	0.29845	278.31	$10^{-3}$
8	Trimethoprim	0.008550295151	0.26425	290.32	$10^{-3}$
9	Sulfachloropyridazine	0.1377701226	0.40264	284.72	$10^{-3}$
10	Carbamazepine	0.04230344829	0.31795	236.269	$10^{-3}$

Table 3.1: Contaminants model parameters [25].

Let us point out that all micro-pollutants were identified as problematic by KWR in terms of convergence of the numerical schemes they have used [25]. Below, we provide some general information about the contaminants, described in 3.1:

- Natural organic matter (NOM) is a complex mixture of thousands of carbon-based organic compounds, found in water. It is matter, which usually comes from decaying plants and animals and their waste products in the environment [23].
- Furosemide is a medication used to treat fluid build-up in the body's tissues, caused by heart, liver, and kidney diseases. It may also be used for the treatment of high blood pressure [24].
- Cortisol is a steroid hormone. When used as a medication, it is known as hydrocortisone. It is produced by many animals in response to stress and low blood-glucose concentration [18].

- Ketoprofen, Diclofenac, and Phenazone are non-steroidal anti-inflammatory drugs [27], [21], [30].
- Carbamazepine is an anticonvulsant medication, used primarily in the treatment of epilepsy and neuropathic pain [17].
- Sulfachloropyridazine is a broad spectrum antibiotic, used in veterinary medicine and in the swine, cattle and poultry farming [31].
- Trimethoprim is widespread antibiotic, used in treatment of several infections [33], and Pentoxifylline is worldwide used pain-reducing medical [29].

For simplicity, each of the contaminants is associated with a number in Table 3.1, which is often used further in the document instead of the specific contaminant name.

### 3.1 Qualitative results for the process of adsorption

In this section, we simulate the adsorption properties of the contaminants in Table 3.1. Thus, we validate the robustness of the fully-implicit and discuss the qualitative nature of the model solutions of (1.8), (1.9), (1.11) and (1.8), (1.10), (1.11). We may note that all the experiments in the present section are conducted using the fully-implicit scheme (2.2). The reason is that, as we shall discuss in Section 3.4, it is much more efficient for small values of  $\gamma$ . Let us further note that, after solving the model in nondimensional quantities, the reverse change is made and in all figures results are given in the corresponding physical quantities.

#### 3.1.1 Single-solute modelling

Firstly, we shall focus on the process of a single-solute adsorption using two approaches of representing the load function—the classical Freundlich isotherm (1.9) and SIAS model (1.10). The comparison between these two approaches will serve as a transition to the more general problem of modelling multi-solute adsorption.

For all the experiments in this subsection two contaminants are used—natural organic matter (NOM) and a micro-pollutant, namely Furosemide, with corresponding parameters in the first two rows of Table 3.1.

##### Freundlich isotherm

**Experiment 1.** We consider first the case of only NOM in the water. The results for the concentration and the load, obtained solving (1.8), (1.9), and

(1.11) numerically, are presented in Figure 3.1 and Figure 3.2, respectively. Results seem physically plausible from a qualitative point of view. As time progresses, the filter gets exhausted. Close to the inlet of the filter, there is an expanding area of saturated carbon particles that cannot adsorb any more of the pollutants. Furthermore, as shown by physical experiments, filters are changed in about two years [25], which is consistent with the results, we obtain here.

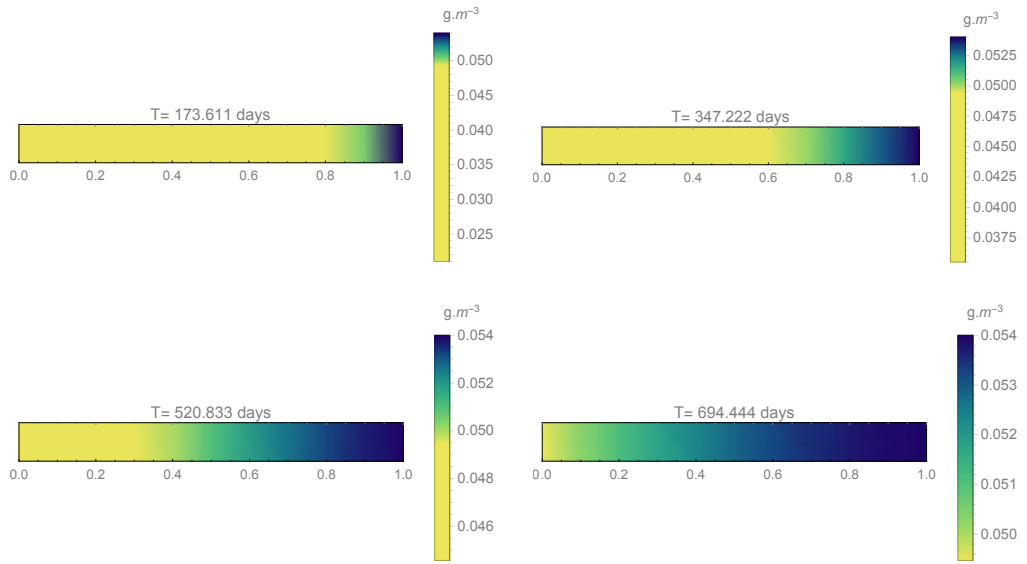


Figure 3.1: **Experiment 1.** Single-component adsorption with Freundlich isotherm. Results for the concentration  $c$  for NOM.

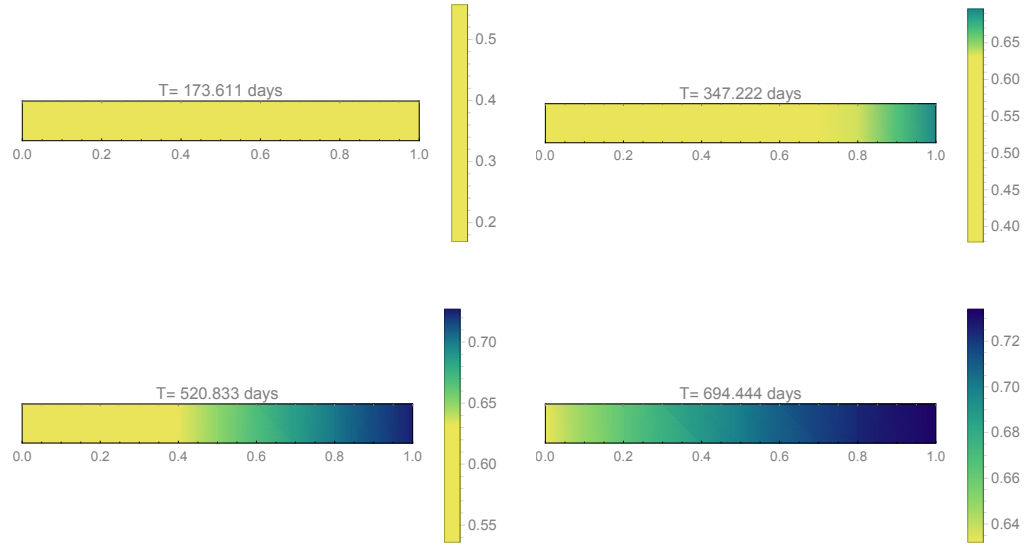


Figure 3.2: **Experiment 1.** Single-component adsorption with Freundlich isotherm. Results for the load  $q$  for NOM.

**Experiment 2.** Next, we choose a micro-pollutant, namely Furosemide. The results for its concentration and load are presented in Figure 3.3 and Figure 3.4, respectively. As one can see, it takes more time for the micro-pollutant to exhaust the filter bed, which is natural because of the smaller size of its particles, and, thus, the better adsorption properties. The lower input concentration of the micro-pollutant should also be considered here.

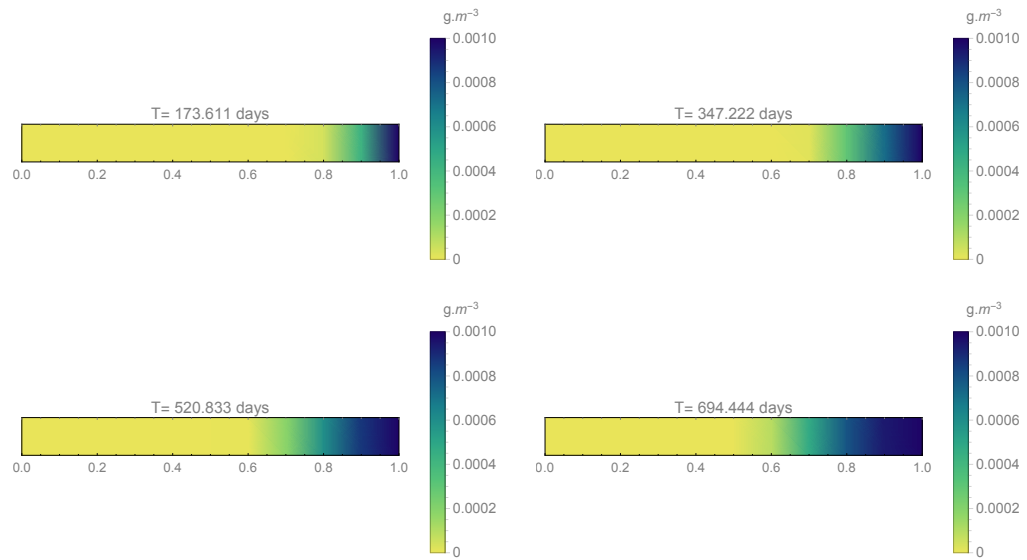


Figure 3.3: **Experiment 2.** Single-component adsorption with Freundlich isotherm. Results for the concentration  $c$  for Furosemide.

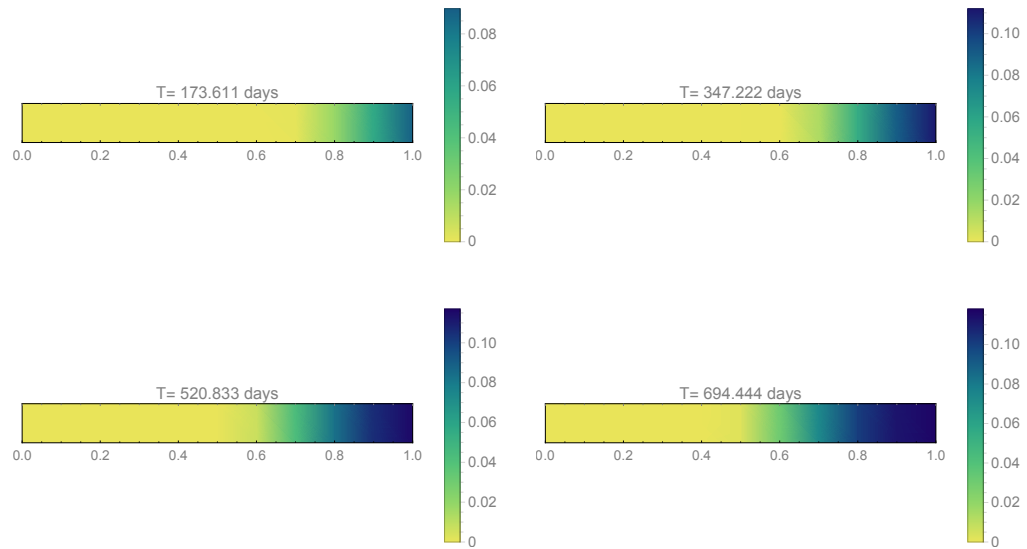


Figure 3.4: **Experiment 2.** Single-component adsorption with Freundlich isotherm. Results for the load  $q$  for Furosemide.

## SIAS model

Next, we repeat the simulations from Experiments 1 and 2, but this time, using SIAS model, i.e., we solve (1.8), (1.10), and (1.11).

**Experiment 3.** In Figures 3.5 and 3.6, results for concentration and load of NOM at the last time layer (i.e.,  $T = 6$ ) using SIAS model are presented (on the left) and a comparison with the respective results obtained with the Freundlich isotherm (Experiment 1) are given on the right. As expected, the outputs from the two load models are indistinguishable. Therefore, SIAS model can indeed be considered as a generalization of the Freundlich isotherm for multiple solutes.

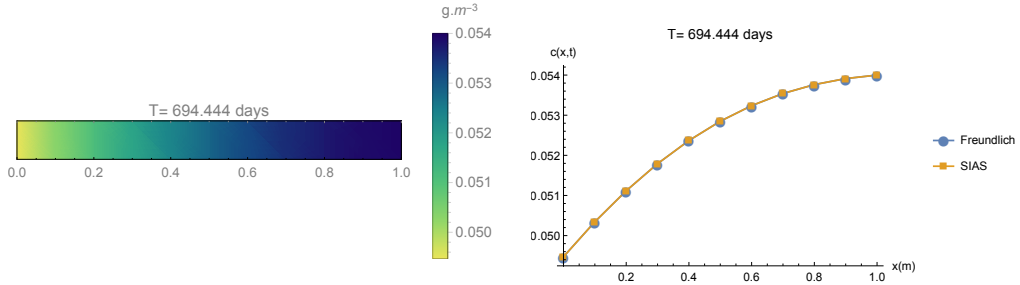


Figure 3.5: **Experiment 3.** Single-component adsorption with SIAS. Results comparison for the concentration  $c$  for NOM at the last time layer.

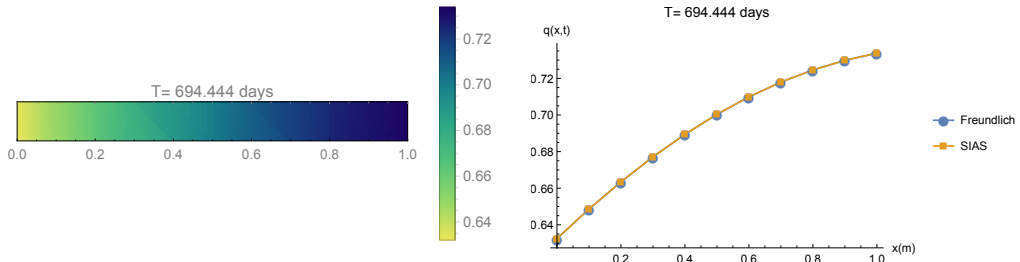


Figure 3.6: **Experiment 3.** Single-component adsorption with SIAS. Results comparison for the load  $q$  for NOM at the last time layer.

**Experiment 4.** It can be seen from Figures 3.7 and 3.8 that the results obtained using Freundlich isotherm (Experiment 2) and SIAS (i.e. solving (1.8), (1.10), (1.11)) are indistinguishable for the micro-pollutant as well.

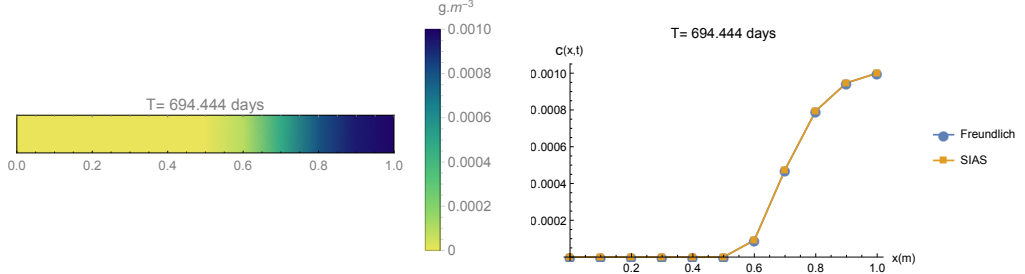


Figure 3.7: **Experiment 4.** Single-component adsorption with SIAS. Results comparison for the concentration  $c$  for Furosemide at the last time layer.

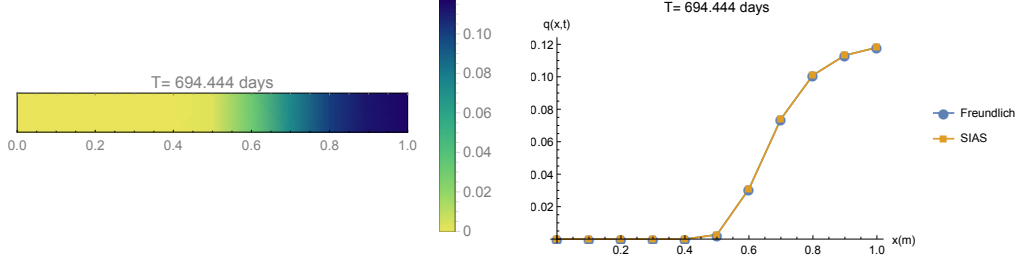


Figure 3.8: **Experiment 4.** Single-component adsorption with SIAS. Results comparison for the load  $q$  for Furosemide at the last time layer.

### 3.1.2 Multi-solute adsorption modelling

Our primary purpose was to generalize the approach to the multi-component case. We use SIAS to model the adsorption onto a carbon filter of up to ten contaminants present in the water—natural organic matter and nine pharmaceutical micro-pollutants, widespread in domestic and industrial water treatment. Thus, we solve the model (1.8), (1.10), and (1.11), using the fully-implicit scheme. Model parameters, used in each of the simulations in the present section, are shown in Table 3.1.

#### Two-component adsorption

**Experiment 5.** As an introduction to the multi-component adsorption, we shall use simultaneously the two pollutants, NOM and Furosemide, used in Experiments 1 to 4. The time evolution of the process is illustrated in Figures 3.9 and 3.10 for NOM and Figures 3.11, 3.12 for the micro-pollutant.

The results for NOM show that its concentration in the case of multi-component

adsorption is higher, compared to its concentration in the single-component case that we computed in Experiment 1 (see Figure 3.9b), which is a clear indicator that the two contaminants compete with each other for adsorption sites. This statement is confirmed by the results, obtained for the load on the carbon, which is lower in the case of two contaminants, especially at the end of the second year of operation as illustrated in Figure 3.10b.

The results for Furosemide concentration, in turn, show that micro-pollutant particles have reached further throughout the filter bed, compared to the single-component case (compare Figure 3.11a and Figure 3.3), which means, that the filter passes particles more easily. From Figure 3.11b, one can see that the concentration of micro-pollutant is significantly higher in the two-component case, and evidently, at the end of the second year, the effluent concentration of Furosemide is non-zero. The load on the carbon for Furosemide in the two-component case, is very low, even at the inlet of the filter (Figure 3.12). This is another argument in favour of the hypothesis that the two contaminants hinder each other in the adsorption process.

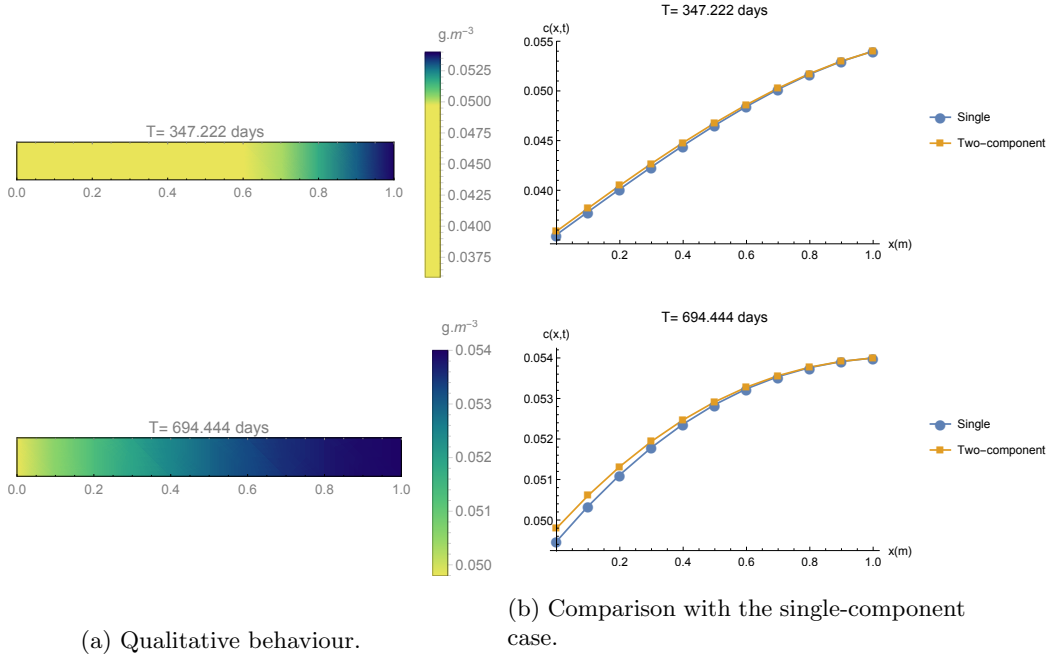


Figure 3.9: **Experiment 5.** Two-component adsorption. Results for the concentration  $c$  for NOM.

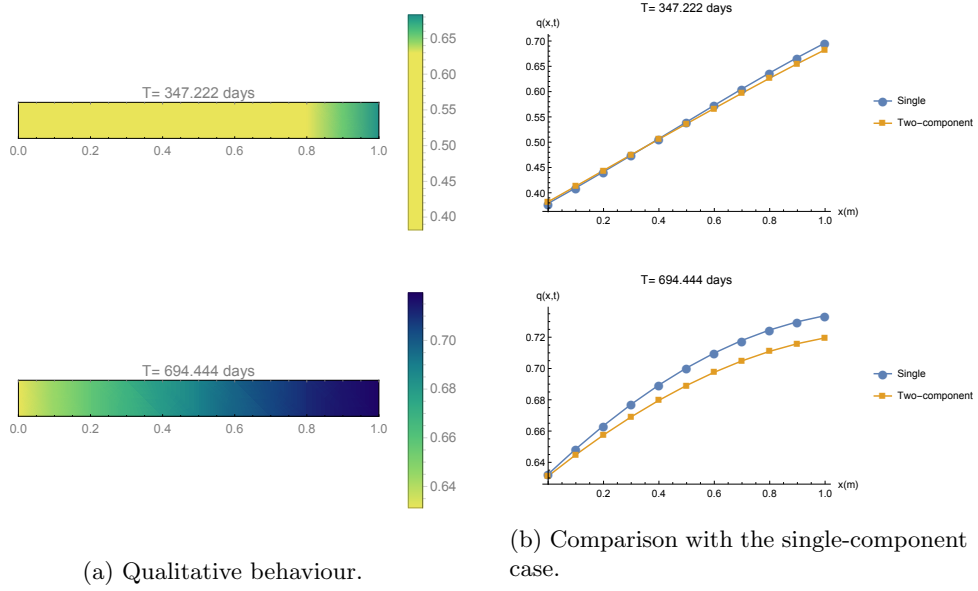


Figure 3.10: **Experiment 5.** Two-component adsorption. Results for the load  $q$  for NOM.

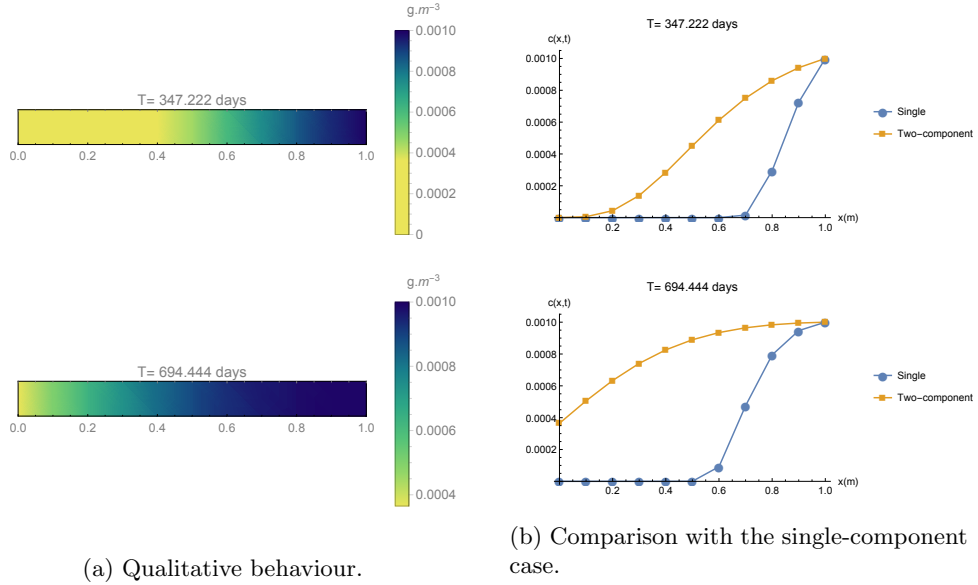


Figure 3.11: **Experiment 5.** Two-component adsorption. Results for the concentration  $c$  for Furosemide.

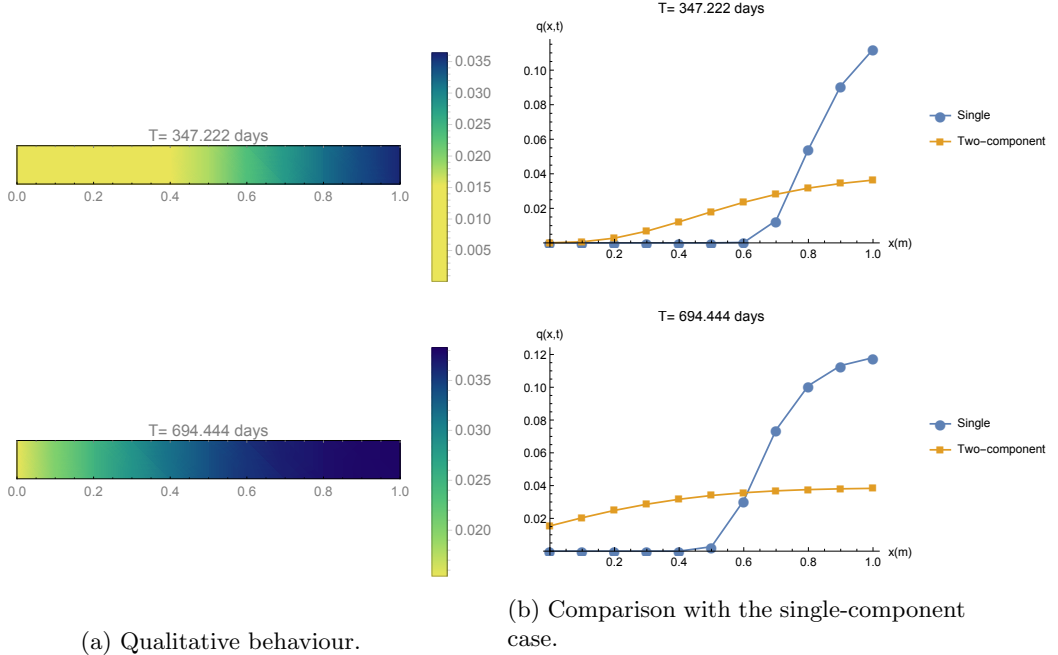


Figure 3.12: **Experiment 5.** Two-component adsorption. Results for the load  $q$  for Furosemide.

### Ten-component adsorption

**Experiment 6.** Using the scheme (2.2), we successfully managed to simulate the process for 10 contaminants in the water by solving the corresponding system of 20 PDEs. Results for NOM and Furosemide are presented again in order to make a comparison with the previous cases in Figures 3.13 to 3.16. We can conclude that the presence of more pollutants in the water does not affect significantly the behaviour of NOM (compare Figures 3.9 and 3.13). However, it makes adsorption less effective for Furosemide, considering the significant decrease in adsorbed amounts (compare Figures 3.12 and 3.16). Something more—the concentration of Furosemide becomes so large, that even in the middle of the first year of operation, the process of desorption is observed. Note that near the outlet, the concentration is higher than the concentration at the inlet (Figures 3.15b, 3.15c, 3.15d). This process is discussed in more detail in Section 3.3.

The other two contaminants that we consider as representative from this experiment are Phenazone (6) and Trimethoprim (8). These two contaminants not only differ significantly from NOM and Furosemide, but from each other. Phenazone, on the one hand, has very low concentration at the outlet even at the end of the second year (Figure 3.17), compared to other contaminants, and respectively very small quantity of it is being adsorbed there onto the carbon

(Figure 3.18). These observations tell us that Phenazone has high adsorption capacity. Trimethoprim (8), on the other hand, shows very poor adsorbability (Figures 3.19 and 3.20). Even in the early stages of the process, its concentration at the outlet is almost equal to the inlet. This observation is confirmed by the results for the load—its values are extremely low during the whole process. In fact, Phenazone (6) is characterized with small molar weight, but large Freundlich parameters, whereas Trimethoprim (8) corresponds to very low values of Freundlich parameters (Table 3.1). This fact seems like a reasonable explanation for their behaviour—Freundlich isotherms describe the adsorption capacity for a specific substance, so higher values of Freundlich constants mean higher adsorption capacity.

We do not present the results for the rest of the contaminants here, because they are qualitatively similar to one of the presented four. We shall discuss them, however, in terms of their so-called breakthrough curves in the next section.

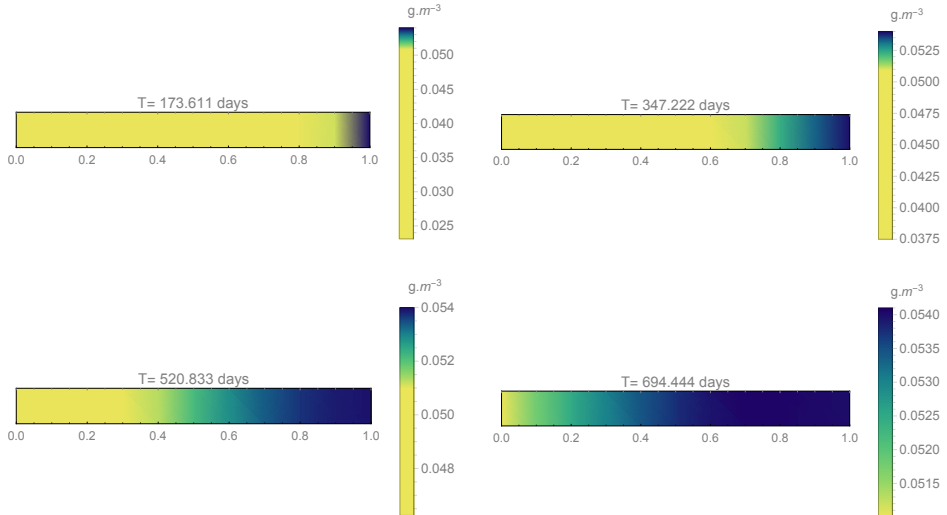


Figure 3.13: **Experiment 6.** Ten-component adsorption. Results for the concentration  $c$  for NOM.

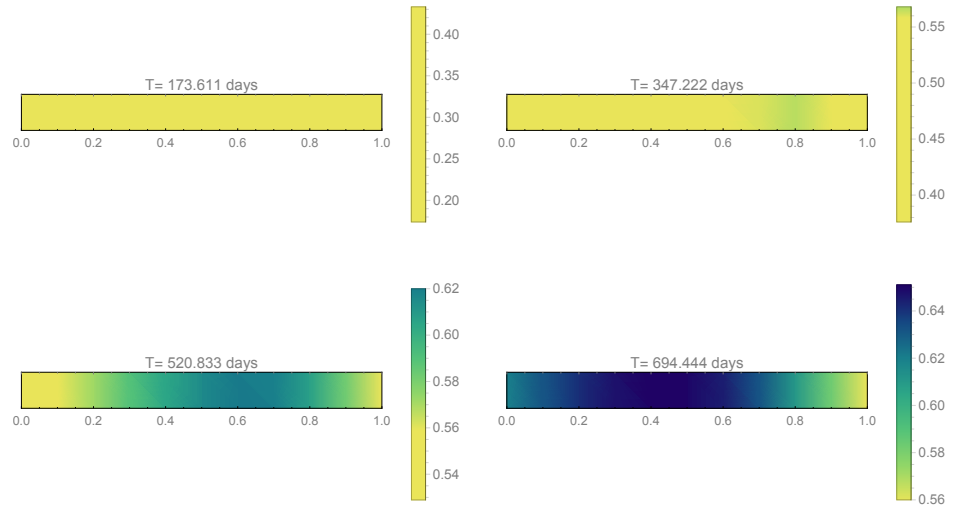


Figure 3.14: **Experiment 6.** Ten-component adsorption. Results for the load  $q$  for NOM.

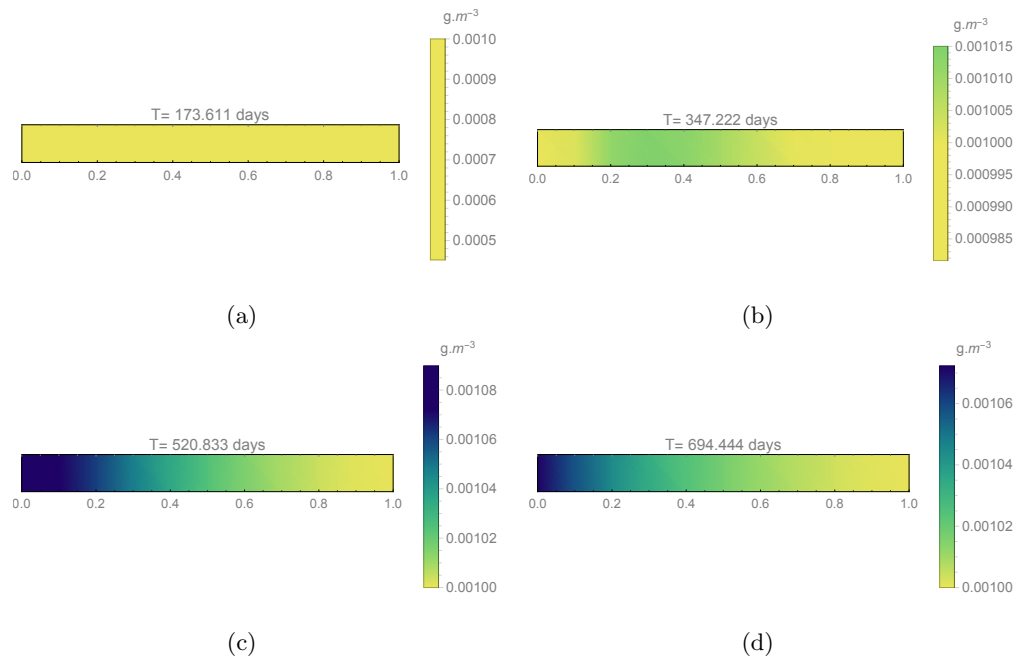


Figure 3.15: **Experiment 6.** Ten-component adsorption. Results for the concentration  $c$  for Furosemide.

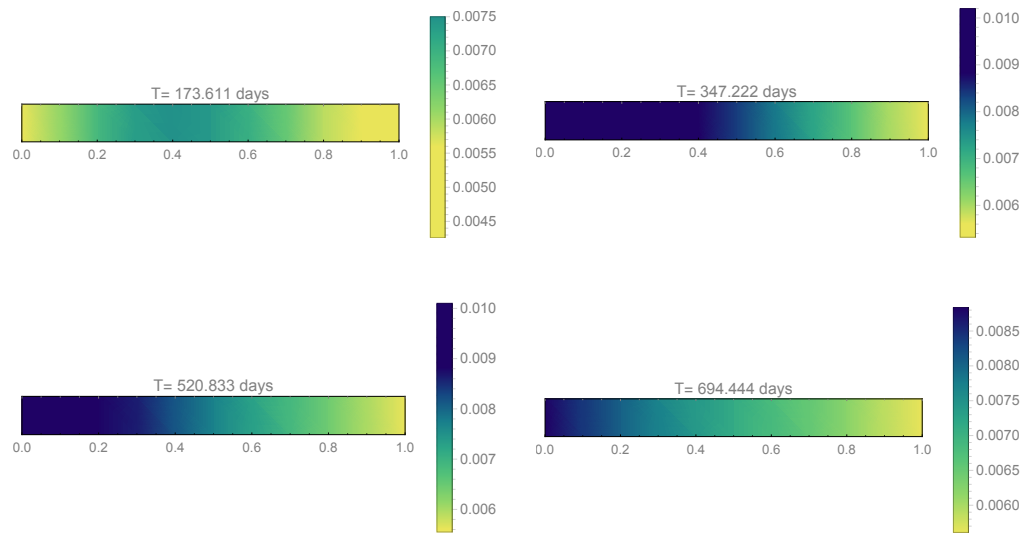


Figure 3.16: **Experiment 6.** Ten-component adsorption. Results for the load  $q$  for Furosemide.

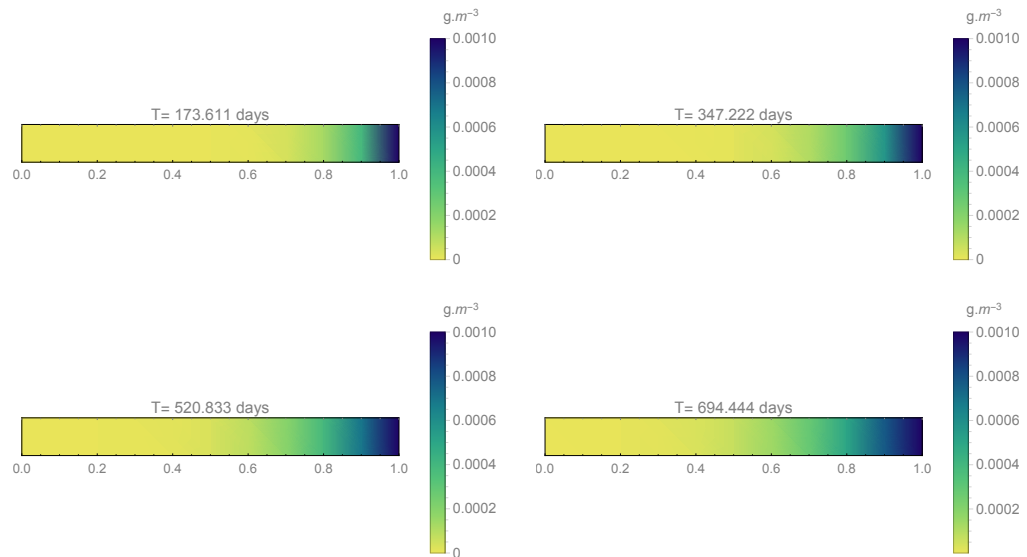


Figure 3.17: **Experiment 6.** Ten-component adsorption. Results for the concentration  $c$  for Phenazone.

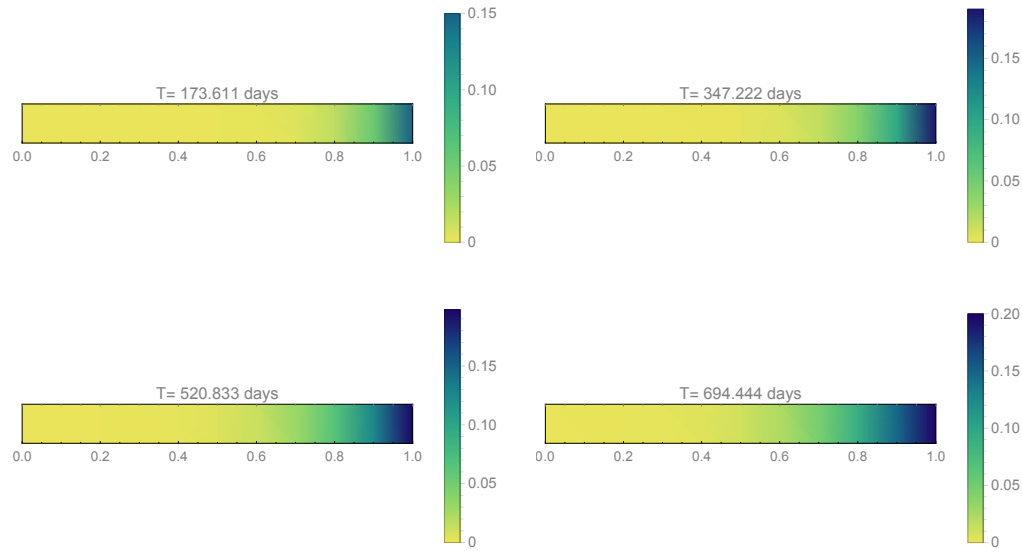


Figure 3.18: **Experiment 6.** Ten-component adsorption. Results for the load  $q$  for Phenazone.

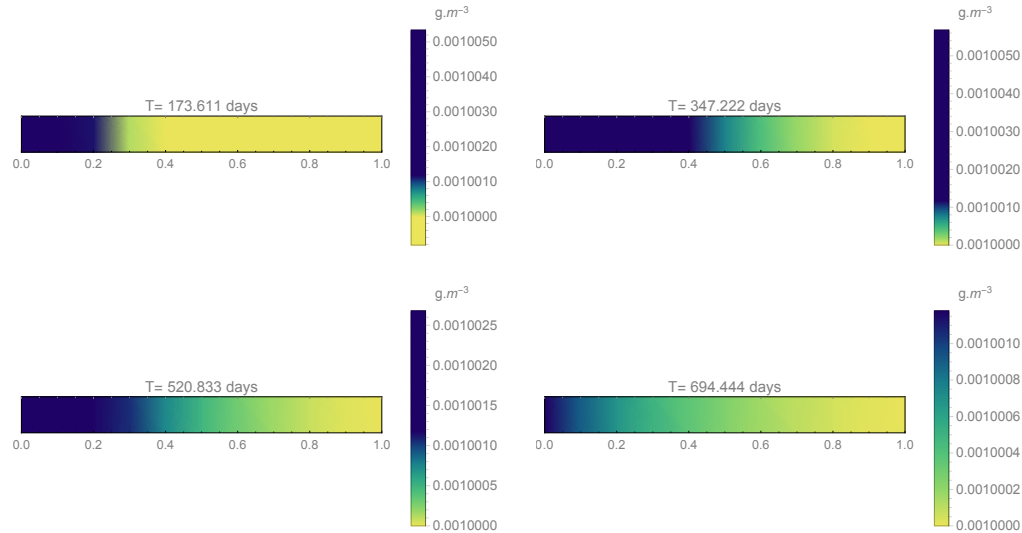


Figure 3.19: **Experiment 6.** Ten-component adsorption. Results for the concentration  $c$  for Trimethoprim.

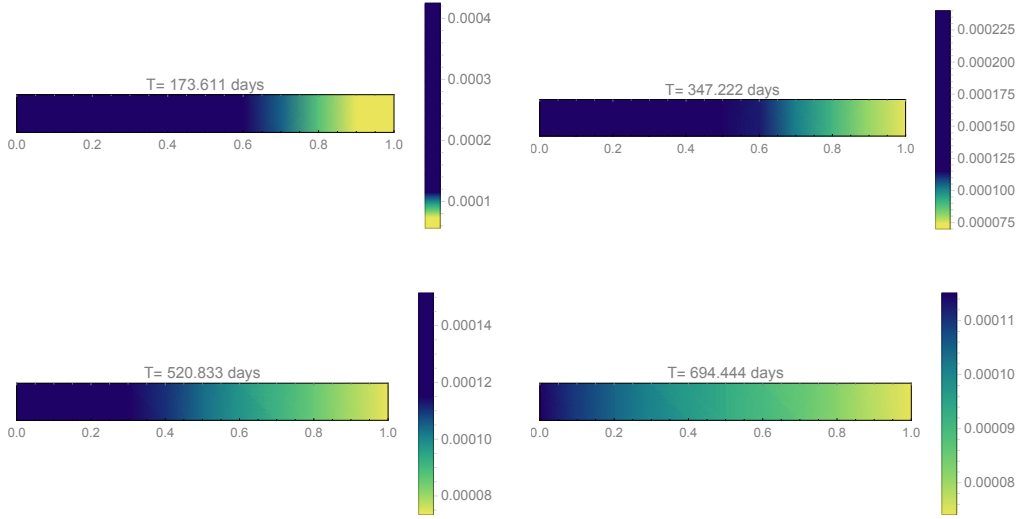


Figure 3.20: **Experiment 6**. Ten-component adsorption. Results for the load  $q$  for Trimethoprim.

### 3.2 Breakthrough curves

The most important reason for modelling the process of adsorption in water treatment applications is to determine the moment of filter-bed exhaustion, since the process of regeneration/reactivation of a carbon filter's adsorption abilities is a very expensive procedure (see the Appendix). The exhaustion of a filter is closely related to the term “breakthrough”. At some point of time after the beginning of the purifying procedure, the mass transfer zone (i.e., the particular part of the filter bed, at which actual adsorption takes place, since the material above this zone is already saturated, see the Appendix) reaches the end of the carbon bed (Figure 3.21). Subsequently, some adsorbate leaves the filter with the effluent, which, of course, is not desirable. This is called breakthrough. This concept is formalized by considering the so-called **breakthrough curves**, which represent the ratio  $c_{outlet}/c_{inlet}$ , which we shall further denote for brevity by  $c/c_0$ , as a function of time.

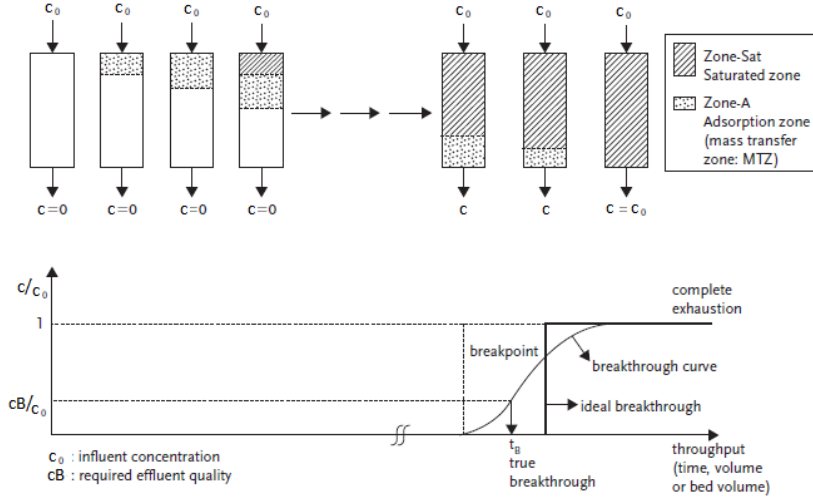


Figure 3.21: Breakthrough characteristics in a GAC adsorber [3].

Prior to breakthrough, the concentration of adsorbate in the effluent is nearly zero, then it increases as the mass transfer zone gets closer to the outlet. Theoretically, this increase can continue until the moment in which the effluent concentration becomes equal to the influent one. However, depending on the specific contaminant, even tiny concentrations, present at the effluent, might not be acceptable.

In this section, we present breakthrough curves for contaminants used in our experiments. In Figures 3.22, 3.23, 3.24, each colour corresponds to different number of contaminants, present in the water. For example, 3 means that contaminants 1, 2, 3 were assumed to be present in the water; 4 means that contaminants 1, 2, 3, 4 are present in the water, etc.

**Experiment 7.** In Figure 3.22, the breakthrough curves for NOM in the case of single-solute adsorption and 4- and 10-contaminant adsorption, are compared. Seemingly, the number of micro-pollutants present in the solute, does not affect significantly the behaviour of NOM, which is natural, because of its higher input concentration.

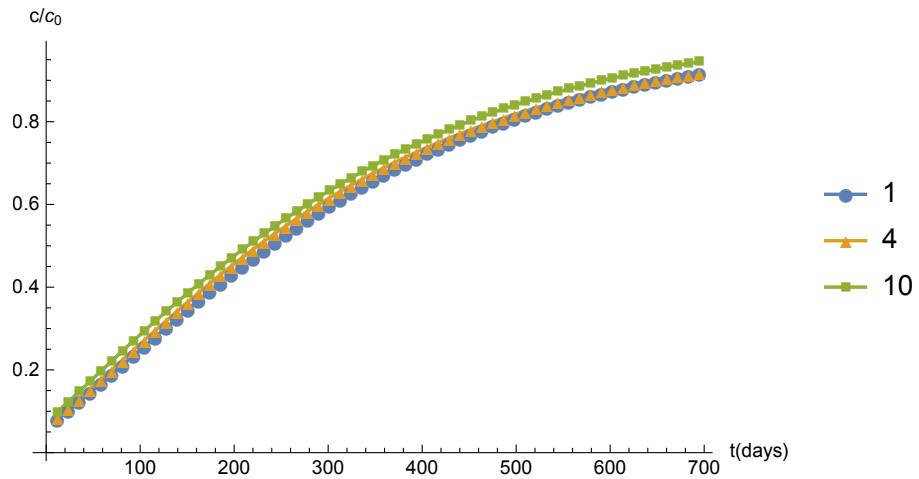


Figure 3.22: **Experiment 7.** Breakthrough curves for NOM in case of 1, 4, and 10 contaminants.

**Experiment 8.** The behaviour of the first micro-pollutant, Furosemide (2), is much more dynamic (Figure 3.23). In the single-contaminant case, even after two years of operation, the concentration of contaminant at the effluent is still indistinguishable from zero. With the presence of NOM in the water, at the middle of the second year of operation, the filter passes some small quantity of the micro-pollutant at the effluent. With the increment of number of contaminants, the moment of breakthrough (we can see that at some point in time,  $c/c_0$  becomes larger than 0.1) occurs earlier and earlier, reaching about 50 days of operational time in the ten-contaminants case.

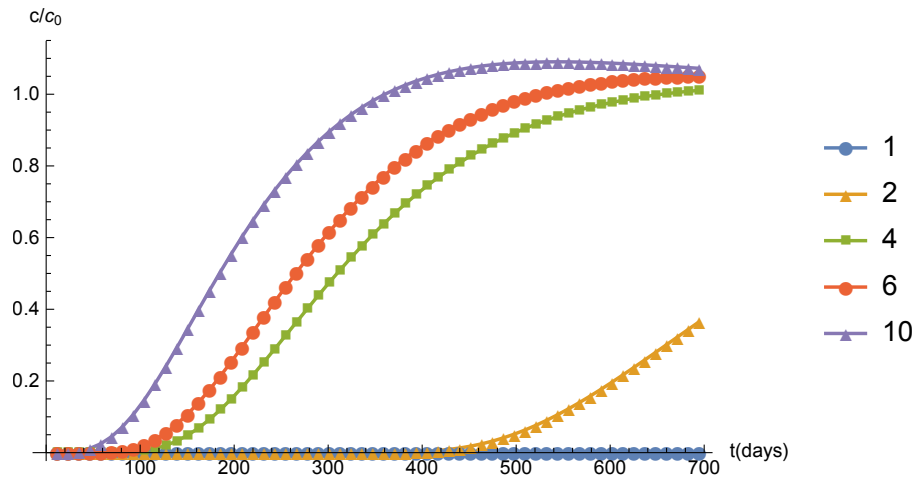


Figure 3.23: **Experiment 8.** Breakthrough curves for Furosemide in case of 1, 4, 6, and 10 contaminants.

**Experiment 9.** Breakthrough of Diclofenac (Figure 3.24) is very similar to this of Furosemide (Figure 3.23). Probably this similarity is closely related to the fact that Freundlich parameters of these two micro-pollutants have very close values.

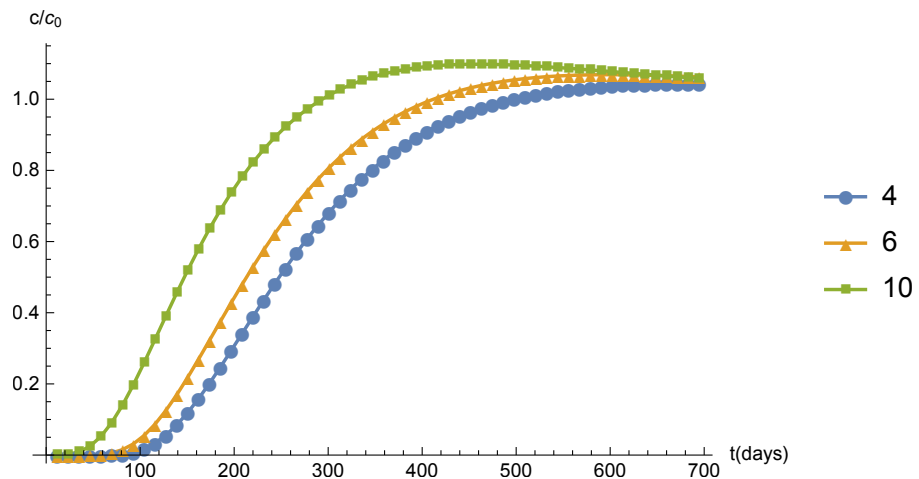


Figure 3.24: **Experiment 9.** Breakthrough curves for Diclofenac in case of 4, 6 and 10 contaminants.

Let us note that in both Experiments 8 and 9,  $c/c_0$  becomes greater than 1 for some time interval in the case of 10 contaminants. This is

connected with the process of desorption, which we shall discuss in the next section.

**Experiment 10.** In Figure 3.25, there is a representative example of another type of breakthrough—breakthrough of a micro-pollutant Phenazone with relatively high values of single-solute Freundlich parameters. It differs a lot from the breakthrough of micro-pollutants like Furosemide and Diclofenac, which, in turn, have greater values of these parameters, as well as a greater molar weight. The adsorption of Phenazone is very intensive, as can be seen in Figure 3.25. Even in the case of ten contaminants, after two years of operation, the concentration of pollutant at the effluent is still negligible, compared to the inlet.

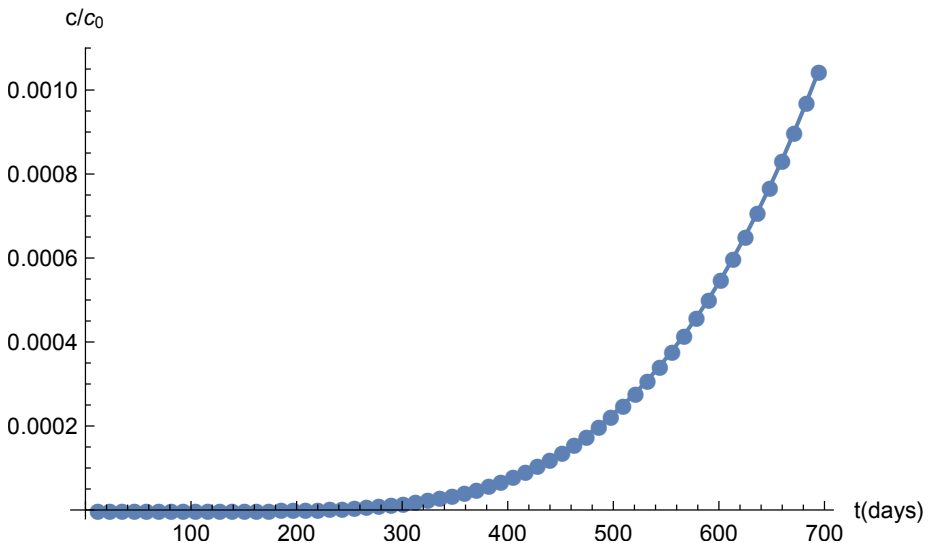


Figure 3.25: **Experiment 10.** Breakthrough curve for Phenazone in case of 10 contaminants.

**Experiment 11.** In Figure 3.26, a comparison between the breakthrough curves of all the ten contaminants, used in our experiments, in the process of their simultaneous adsorption is presented. Each contaminant is denoted with its corresponding number from Table 3.1. They can be generally divided in four groups, according to their breakthrough behaviour:

- Natural organic matter (1) differs significantly from the micro-pollutants, having relatively high concentration values at the effluent at an early stage of the process.
- Furosemide (2), Diclofenac (3), Cortisol (4), Pentoxifylline (7), and Carbamazepine (10) form the biggest group among the tested micro-pollutants.

These contaminants show “regular” adsorption properties. Their loading on the carbon increases regularly and smoothly, reaching critical values at the range between the middle and the end of the first year of operation. What is also interesting about this group of contaminants is that they give us the opportunity to observe the reverse process—desorption, which is discussed in Section 3.3. Here, we identify it as the fact that  $c/c_0$  becomes larger than 1.

- Ketoprofen (5), Phenazone (6), and Sulfachloropyridazine (9) are characterized with very high levels of adsorption. Until the end of the second year, their concentrations at the effluent are almost negligible.
- Trimethoprim (8) is the only contaminant in this last group. This contaminant seems like it is not being adsorbed at all. Even during the first few days of filter operation its concentration at the effluent is almost equal to the initial one. The hypothesis that contaminant (8) is hardly being adsorbed is supported by the fact that for this contaminant process of desorption does not occur, despite the large concentration values in the filter. This behaviour can be explained by the significantly smaller values of the Freundlich constants of this contaminant.

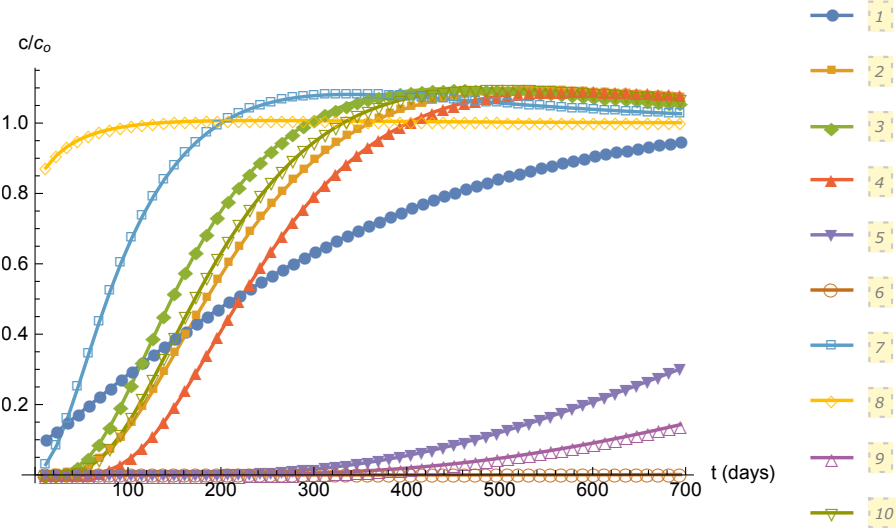


Figure 3.26: Breakthrough curves for all contaminants in the ten-component case.

What we can conclude from our numerical experiments, is that Freundlich parameters have a great influence on the adsorption behaviour of contaminants not only in the single-component case, but in the multi-component, as well.

We observed that the greater the values of Freundlich constants, the better the adsorption.

### 3.3 Regarding the reverse process: desorption

Desorption is a phenomenon, whereby a substance is released from or through a surface. The process is the opposite of sorption (a term that generalizes adsorption and absorption). This occurs in a system being in the state of sorption equilibrium between bulk phase (fluid, i.e., gas or liquid solution) and an adsorbing surface (solid or boundary separating two fluids). When the concentration (or pressure) of substance in the bulk phase is lowered, some of the sorbed substance changes to the bulk state [19].

In our numerical experiments with some of the micro-pollutants, we observed the exact same phenomenon—after enough time had passed and the filter had started to exhaust, the concentrations of contaminant in the bulk phase (water) become lower than the concentration inside the carbon particles (**many organic substrates tend to desorb from activated carbon as a result of the reversal of concentration gradient between carbon surface and bulk medium; it is also possible that adsorbed pollutants are displaced by more adsorbable ones [3]**). This imbalance provokes contaminant molecules to move back into the solute. This phenomenon can be observed even on the breakthrough curves in Figure 3.23 and Figure 3.24—the ratio between outlet and inlet concentration becomes larger than 1, meaning that the reverse process has started and the concentration at the effluent of the filter has become greater than the input one.

**Experiment 12.** In Figure 3.27, results for the concentrations of two of the experimental contaminants, namely Furosemide and Diclofenac, in the case of 6- and 10-component adsorption are presented. With dashed line the value of the input concentration of all micro-pollutants, used in the numerical experiments, is denoted, i.e.,  $c_{0,m} = 10^{-3}$ .

Until the moment  $T = 173.611$  days, the process of adsorption is evolving as expected, i.e., close to the inlet of the filter, the concentration of the contaminants is almost equal to the input one and becomes smaller and smaller, with getting closer to the outlet. In the case of ten contaminants, the process of desorption had already started at the end of the first year of operation (at  $T = 347.222$  the concentrations of both contaminants become greater than the input one). By the middle of the second year of operation (at  $T = 520.833$ ), desorption is observable even in the six-contaminant case (all concentration plots are above the dashed line). What is interesting in the ten-contaminant case, is that at the end of the second year, concentration levels of both micro-pollutants are lowered, compared to values at time  $T = 520.833$ . This is an evidence of the fact that the process of adsorption has started again, trying to maintain concentration equilibrium between the bulk phase and the adsorbing surface.

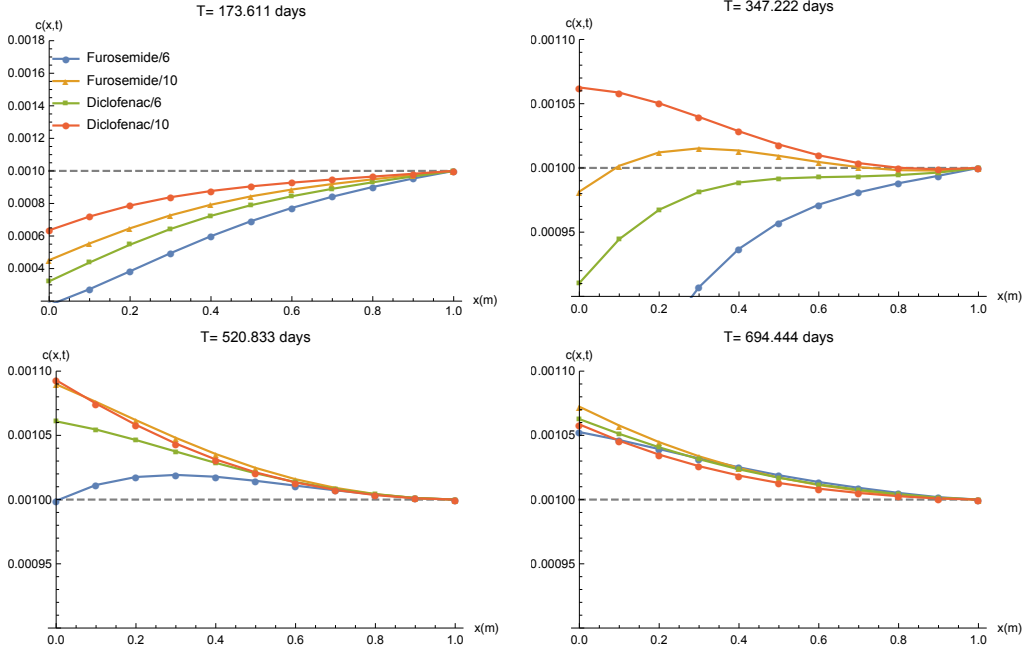


Figure 3.27: The process of desorption of Furosemide and Diclofenac in a multi-component case.

### 3.4 Performance of the numerical schemes

#### 3.4.1 Using a semi-implicit scheme and the influence of $\gamma$

All the parameters, appearing in (1.8) are physically expected to be of similar order to the given values. The parameter  $\gamma$ , however, depends on two others—the diffusion constant of a particular contaminant,  $D_s$ , and the AC particle diameter,  $d_p$ , which can vary in relatively wide ranges and the specific values of those parameters are usually hard to be measured [25]. As discussed in the beginning of the present chapter, some physically sensible values of these parameters that can be found in the literature are  $10^{-15} < D_s < 10^{-13}$  and  $5 \times 10^{-4} < d_p < 5 \times 10^{-3}$ . Therefore, the value of  $\gamma$  can vary in orders of magnitude from  $10^{-9}$  to  $10^{-4}$ . Our experiments showed that the semi-implicit scheme is applicable for values of  $\gamma$  of order up to  $10^{-5}$ —smaller quantities cause severe restrictions on the time discretization step. The reason behind these experiments, however, is that the semi-implicit scheme is much more computationally effective than the fully-implicit one. Therefore, the strengths of the two schemes could be potentially combined, so that the more computationally effective one is chosen for the particular value of  $\gamma$ . In the present paragraph, we provide comparison between the results obtained with the two schemes for  $\gamma = 10^{-4}$ .

and  $10^{-5}$ , as well as an analysis of the effect of this parameter on the model behaviour.

**Experiment 13.** In Figure 3.28, breakthrough curves for NOM are presented for several different values of the parameter  $\gamma$ . As expected, when the value of  $\gamma$  is lower, the evolution of the process is slower. There is a significant difference, especially in the shape of the breakthrough curve, when  $\gamma$  becomes  $10^{-7}$ , compared to greater values of  $\gamma$ .

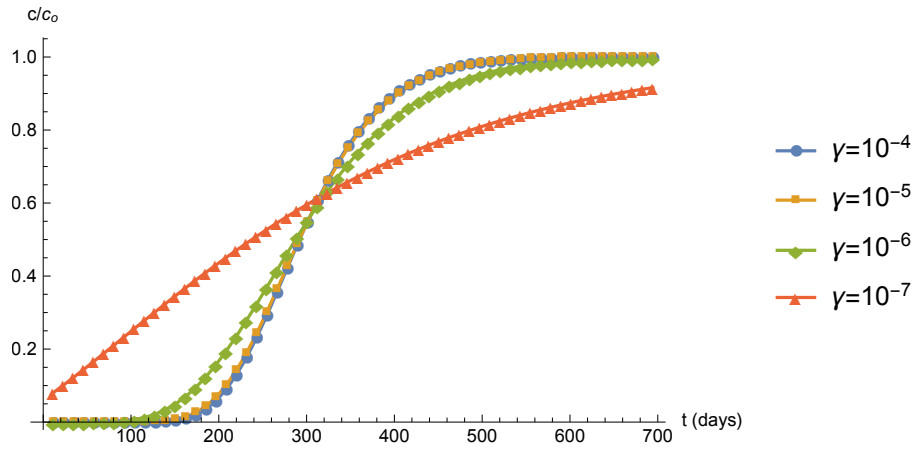


Figure 3.28: **Experiment 13.** Breakthrough curves of NOM for different values of  $\gamma$ .

Numerical experiments for  $\gamma = 10^{-4}$  and  $\gamma = 10^{-5}$  and time-discretization steps  $\tau = 0.1$  and  $\tau = 1$  were conducted, in order to compare the time performance of the proposed numerical schemes (2.1) and (2.2). The results for each experiment are presented in Table 3.2. The corresponding breakthrough curves are all indistinguishable from the ones, depicted in Figure 3.28. We can conclude that, for  $\gamma \geq 10^{-5}$ , the semi-implicit scheme is indeed applicable, and as can be seen from Table 3.2, much more computationally effective. Let us emphasize that numerical experiments that we have carried out have shown that for values of  $\gamma$  about  $10^{-6}$  and lower the time step must be decreased drastically in order to obtain stable results with the semi-implicit scheme.

	Fully-implicit	Semi-implicit
$\gamma = 10^{-4}, \tau = 1$	49.2339	23.7434
$\gamma = 10^{-4}, \tau = 0.1$	419.081	236.544
$\gamma = 10^{-5}, \tau = 1$	5.72524	2.52722
$\gamma = 10^{-5}, \tau = 0.1$	47.2059	24.0866

Table 3.2: **Experiment 13.** CPU time in seconds, needed for adsorption modelling for different values of  $\gamma$  and  $\tau$  using semi-implicit and fully-implicit schemes.

### 3.4.2 Practical estimate of order of convergence

In this subsection, we present an estimate of the order of convergence of the fully-implicit scheme (2.2) that is used in the computation of the majority of the numerical results in the present chapter. For this purpose, we use Runge's method for practical estimation of the order of convergence [6].

**Experiment 14.** For this experiment we construct three nested meshes  $\bar{\omega}_h, \bar{\omega}_{h/2}, \bar{\omega}_{h/4}$ , dividing the computational domain into 10 subintervals, in order to obtain the coarsest mesh,  $\omega_h$ . After computing the model output with each of the three meshes, we compute the order of convergence,  $\alpha$ , at the last time layer, using the following estimate [6]:

$$\alpha = \ln \left| \frac{C_h(x) - C_{h/2}(x)}{C_{h/2}(x) - C_{h/4}(x)} \right| / \ln 2, \quad (3.1)$$

where  $C_h(x)$  is the grid function, corresponding to the approximate solution at the points of the coarsest mesh. Then, if we have  $\alpha(x) \approx \alpha$  at the majority of the common points of the meshes  $\bar{\omega}_h, \bar{\omega}_{h/2}$ , and  $\bar{\omega}_{h/4}$ , we can consider that  $\alpha$  is the actual order of convergence of the numerical scheme. More detailed information about this method can be found in [6].

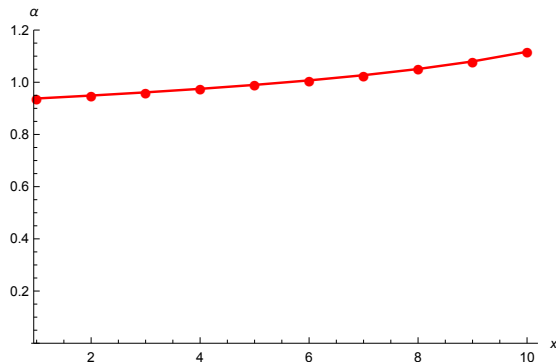


Figure 3.29: **Experiment 14.** A practical estimate of the order of convergence of the fully-implicit scheme (2.2).

In Figure 3.29, values of  $\alpha$ , using the definition (3.1) at the last time layer at each of the points  $x_i, i = 1, \dots, 10$  that are common for the three nested meshes are presented. As one can see, all of the values are approximately equal to 1, so we can conclude that the order of convergence of the fully-implicit scheme (2.2) is equal to the theoretically expected first order.

### 3.4.3 Computational times

Numerical experiments with up to 10 contaminants present in the solute—9 micro-pollutants and natural organic matter, present in the water, were conducted, in order to compare the scalability of the proposed algorithms with respect to the increase of the number of contaminants. From Table 3.3, we can conclude that the fully-implicit scheme solves the system of 20 PDEs, corresponding to 10 contaminants, in less than an hour. Let us further remark that all results were obtained using Wolfram Mathematica. If one uses a compiled programming language like C++, Fortran, Python, etc., the computational times will be significantly lower.

Number	1	2	3	4	5	6	10
Timing (s)	10.7641	384.667	246.918	390.299	640.415	1033.19	1078.65

Table 3.3: CPU time in seconds needed for adsorption modelling with different number of contaminants using the fully-implicit numerical scheme (2.2).

## Chapter 4

# Approximation of the adsorption capacity

As stated in Section 2.3, the complexity of the load function,  $Q$ , defined with (1.10), could cause computational time issues. One possible approach to overcome such problems would be to approximate the problematic function with another one that is much simpler and easier to work with. Spline interpolation theory is a universal approach in such cases. The basics of the theory that we use are given in the Appendix. In this Chapter, we show results of approximating the function  $Q$ , defined with (1.10), with univariate/bivariate splines in the case of one/two contaminants.

### 4.1 Univariate spline interpolation in the one-contaminant case

In this section, we present one possible approach for the approximation of the load functions of NOM and Furosemide (i.e., (1.10), with parameters taken from the first two rows of Table 3.1) in the interval  $[0, 1]$ . Let us discretize the interval by introducing a uniform mesh  $\Omega_{h_s} := \{c_i = ih_s, i = 0, \dots, n_s, n_s = 1/h_s\}$ . We approximate  $Q(c)$  by interpolating it at the mesh nodes with the linear spline  $Q_{I,h_s}(c) \in S_1(c_1, \dots, c_{n_s-1})$ . I.e., we construct (see the Appendix)

$$Q_{I,h_s}(c) = \sum_{i=0}^{n_s} Q(c_i) \phi_i(c), \quad (4.1)$$

where

$$\begin{aligned}\phi_0(c) &= \begin{cases} \frac{c_1 - c}{h_s}, & c \in [c_0, c_1], \\ 0, & c > c_1, \end{cases} \\ \phi_i(c) &= \begin{cases} \frac{c - c_{i-1}}{h_s}, & c \in [c_{i-1}, c_i], \\ \frac{c_{i+1} - c}{h_s}, & c \in [c_i, c_{i+1}], \\ 0, & \text{otherwise,} \end{cases}, \quad i = 1, \dots, n_s - 1, \\ \phi_{n_s}(c) &= \begin{cases} \frac{c - c_{n_s-1}}{h_s}, & c \in [c_{n_s-1}, c_{n_s}], \\ 0, & c < c_{n_s-1}. \end{cases}\end{aligned}\quad (4.2)$$

**Experiment 15.** Let us consider NOM, i.e.,  $Q(c)$  is defined with (1.10) and parameters, taken from the first row of Table 3.1. Let  $h_s = 0.005$ . The load function and its interpolant are depicted in Figure 4.1. The two are indistinguishable.

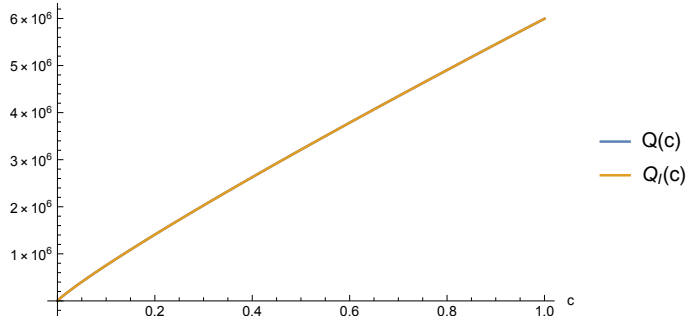


Figure 4.1: **Experiment 15.** Load function of NOM and its linear spline interpolant.

In Figure 4.2, the absolute value of the absolute error between  $Q$  and  $Q_{I,h_s}$  is presented. One can see that the error decreases with the increase of  $c$ . The relative error  $(Q(c) - Q_{I,h_s}(c))/Q(c)$  at concentration values, close to zero, is significant (Figure 4.3). Nevertheless, the error, relative to  $\|Q\|_{L_\infty[0,1]}$  is small. Thus, we proceed by studying numerically the effect of substituting  $Q$  with  $Q_{I,h_s}$  in the model (1.8), (1.10), (1.11). The values for the concentration and load at the last time layer, i.e.,  $T = 6$  in non-dimensional units are depicted in Figures 4.4 and 4.5. As one can see, the result is visually indistinguishable from the one, obtained with the original function  $Q$ . On the other hand, as we shall discuss in the next section, the usage of  $Q_{I,h_s}$  decreases the computational time.

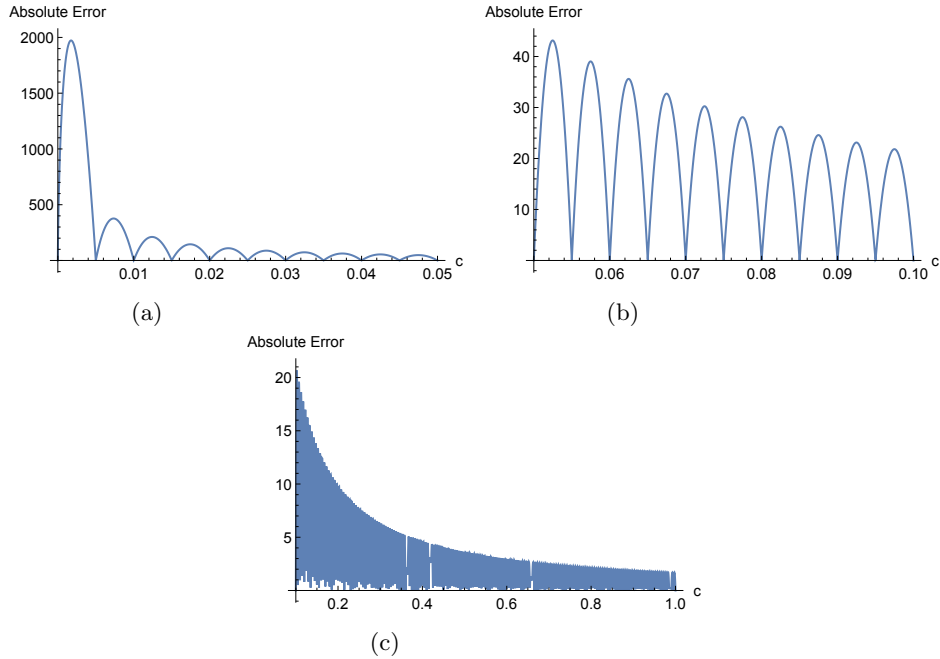


Figure 4.2: **Experiment 15.** Absolute error from linear spline interpolation with step 0.005 for NOM.

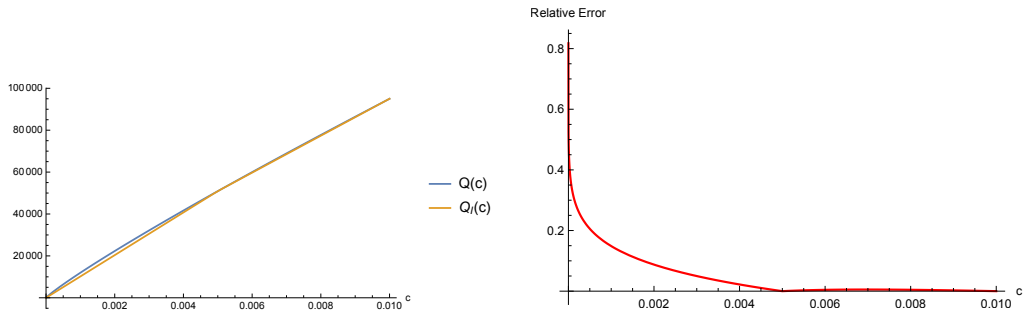


Figure 4.3: **Experiment 15.** Relative error from linear spline interpolation with step 0.005 for NOM in the interval  $[0, 0.01]$

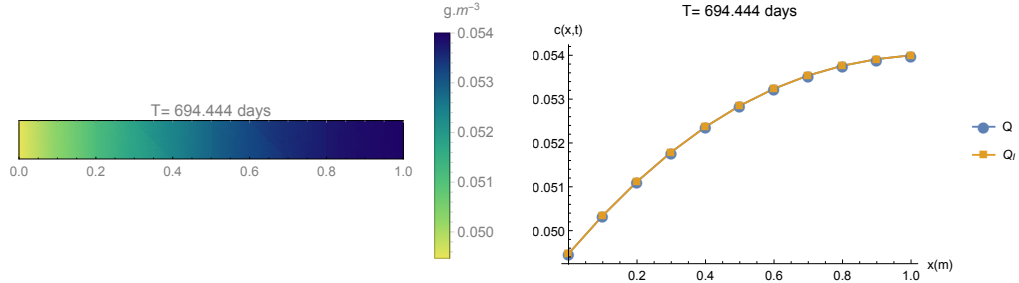


Figure 4.4: **Experiment 15.** Results for the concentration  $c$  for NOM using linear spline interpolation with mesh step 0.005.

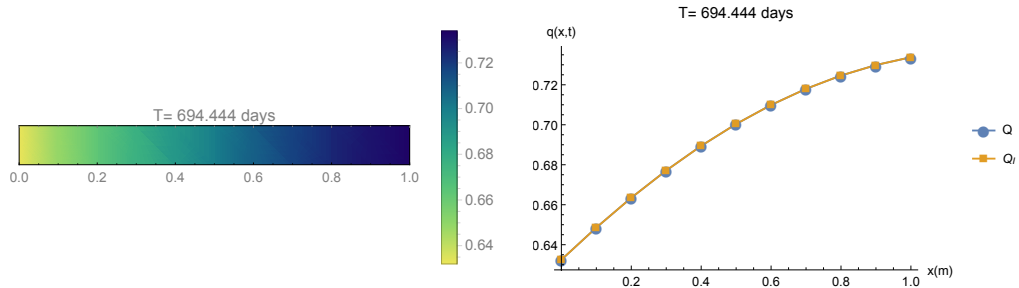


Figure 4.5: **Experiment 15.** Results for the load  $q$  for NOM using linear spline interpolation with mesh step 0.005.

**Experiment 16.** Next, we change the step  $h_s$  with respect to the previous experiment and we choose  $h_s = 10^{-6}$ . The error  $|Q(c) - Q_{I,h_s}(c)|$  is illustrated in Figure 4.6. Decreasing the step about three orders of magnitude, the error decreases of the same order.

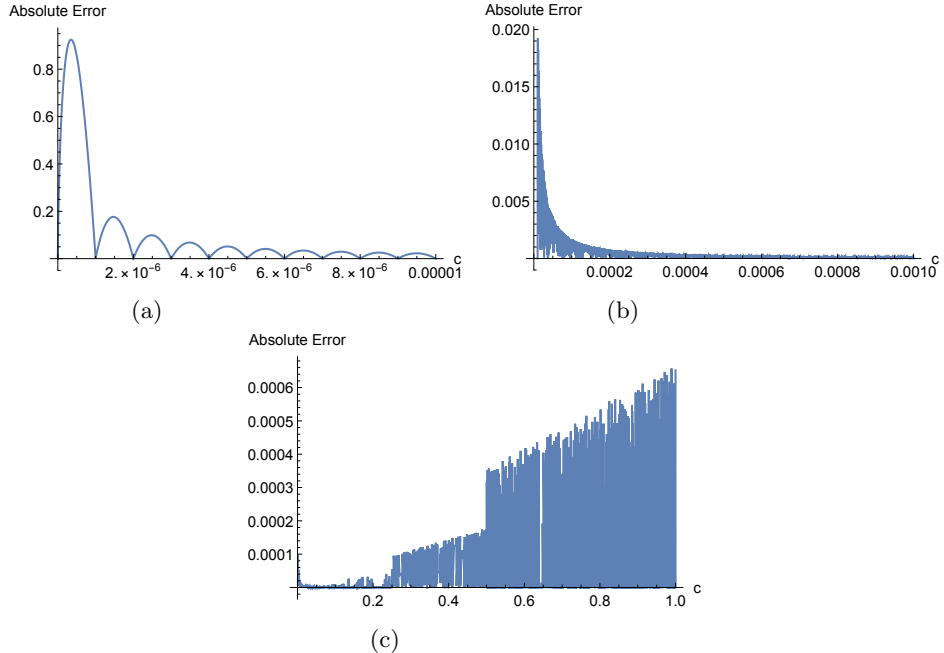


Figure 4.6: **Experiment 16.** Absolute error from linear spline interpolation with step  $10^{-6}$  for NOM.

**Experiment 17.** Let us now consider the micro-pollutant Furosemide, i.e.,  $Q(c)$  is defined with (1.10) and parameters, taken from the second row of Table 3.1. The original load function and its interpolant, using  $h_s = 0.005$ , are also visually indistinguishable in the interval  $[0, 1]$ , as can be seen in Figure 4.7.

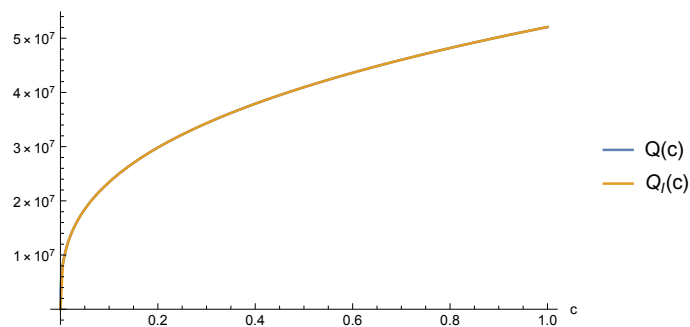


Figure 4.7: **Experiment 17.** Load function of Furosemide and its linear spline interpolant.

In Figure 4.8, the absolute approximation error is given. As one can see from Figure 4.9, the relative error in the vicinity of  $c = 0$  is significantly larger

than the NOM case. Such a result is expected, because of the large value of the derivative of the original function. Nevertheless, substituting  $Q$  in model (1.8), (1.10), (1.11) with  $Q_{I,h_s}$ , the result remains perfectly adequate, as seen from Figures 4.10 and 4.11. Let us further note that if one decreases  $h_s$  to  $10^{-6}$ , the approximation error significantly decreases, see Figure 4.12.

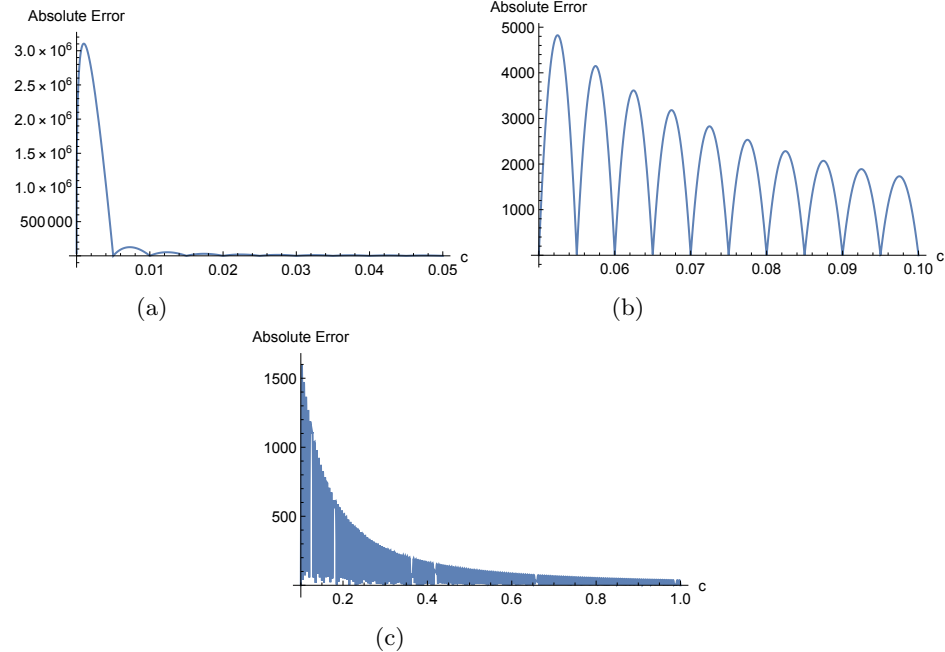


Figure 4.8: **Experiment 17.** Absolute error from linear spline interpolation with step 0.005 for Furosemide.

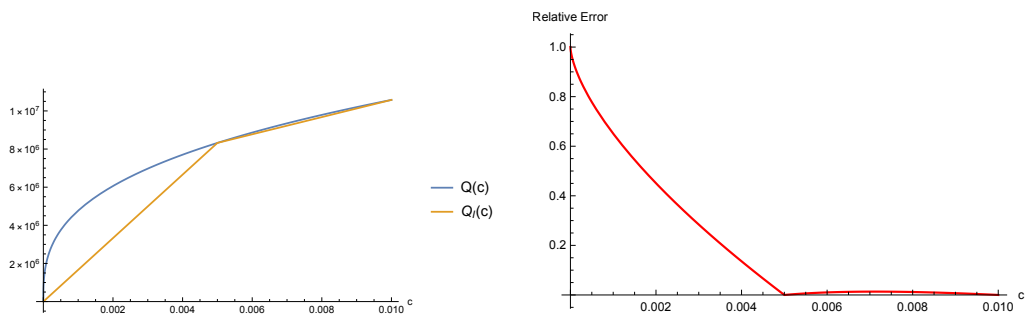


Figure 4.9: **Experiment 17.** Relative error from linear spline interpolation with step 0.005 for NOM in the interval  $[0, 0.01]$

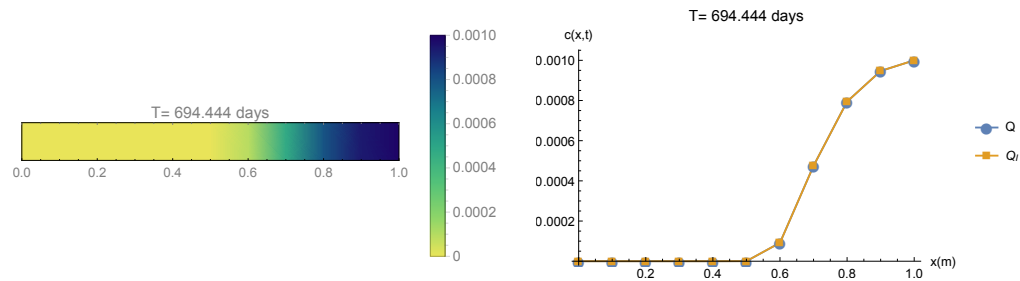


Figure 4.10: **Experiment 17.** Results for the concentration  $c$  for Furosemide using linear spline interpolation with mesh step 0.005.

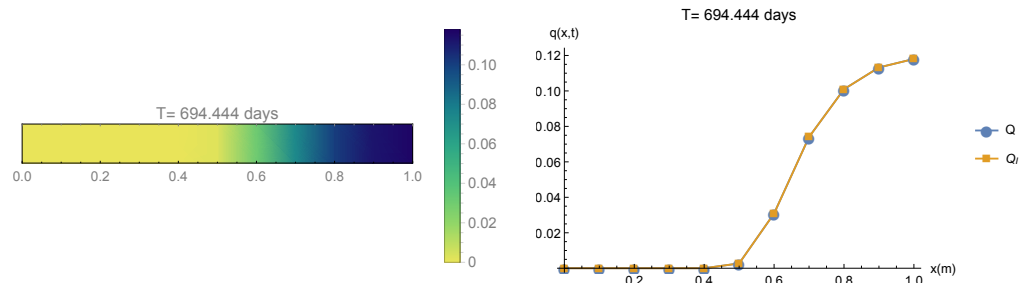


Figure 4.11: **Experiment 17.** Results for the load  $q$  for Furosemide using linear spline interpolation with mesh step 0.005.

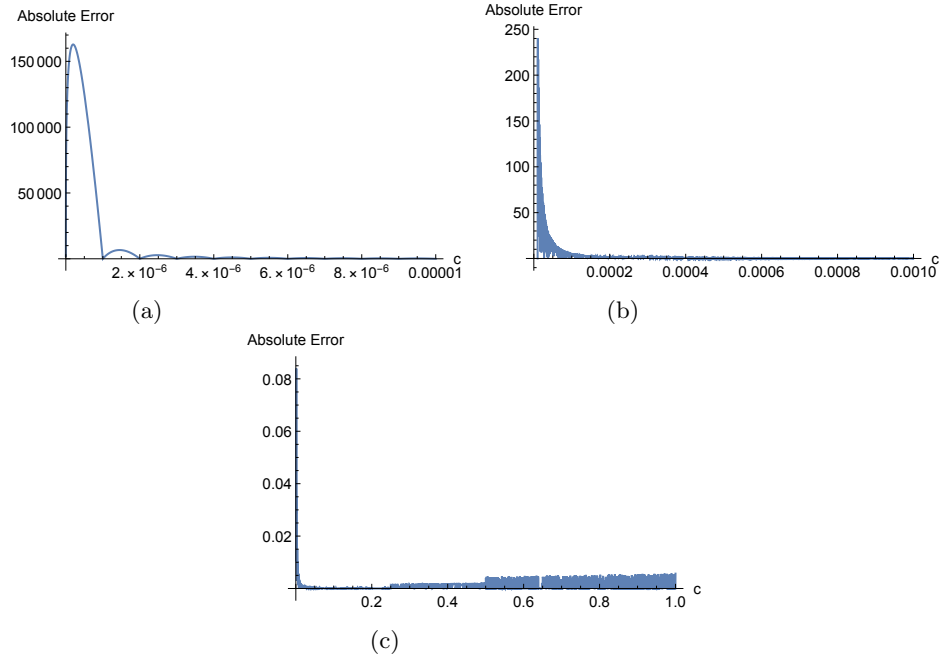


Figure 4.12: **Experiment 17.** Absolute error from linear spline interpolation with step  $10^{-6}$  for Furosemide.

**Experiment 18.** Further, we present numerical results that aim to give some intuition about the convergence of the solution of the differential problem (1.8), (1.10), (1.11) when  $Q_{I,h_s}$  is used (let us denote it by  $C_{Q_I}$ ) to the solution, when the original  $Q$  is used. In Figure 4.13, the values of  $|C - C_{Q_I}|$  at the last time layer for NOM at the mesh nodes are given for  $h_s = 0.005$  and  $h_s = 10^{-6}$ . In Figure 4.14, the corresponding results for Furosemide are depicted. From the numerical results, one can assume a first-order convergence.

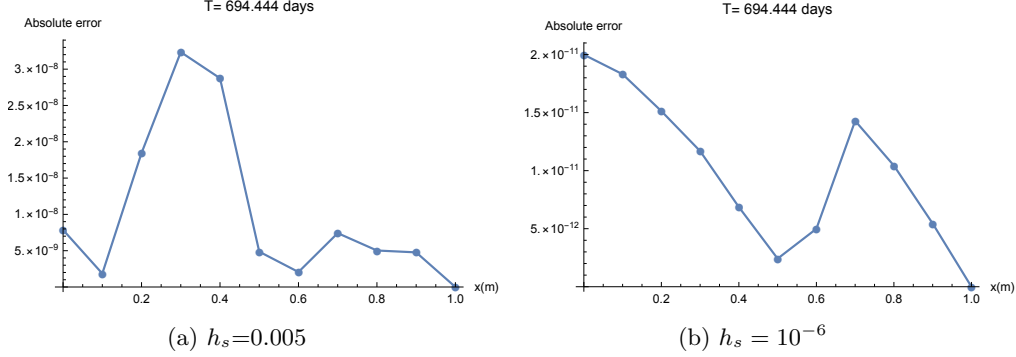


Figure 4.13: **Experiment 18.** Absolute errors between the approximate solutions with spline interpolation and SIAS model for the concentration of NOM.

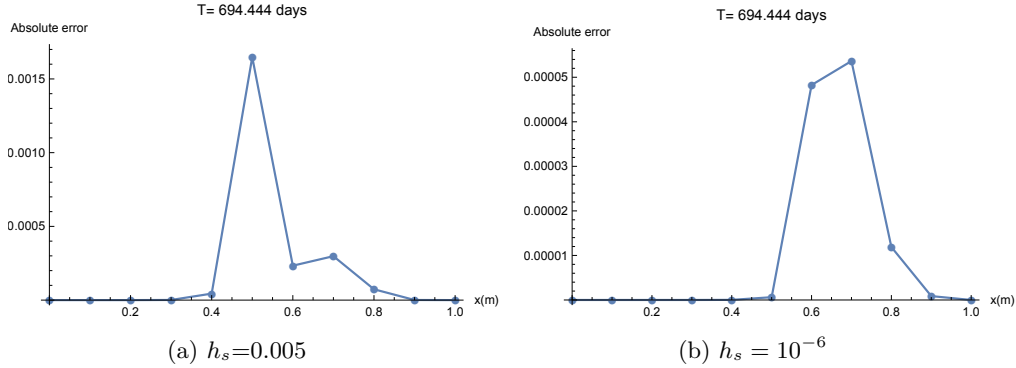


Figure 4.14: **Experiment 18.** Absolute errors between the approximate solutions with spline interpolation and SIAS model for the concentration of Furosemide.

## 4.2 Bivariate spline interpolation in the two-contaminant case

We shall now consider the approximation of the load functions of NOM and Furosemide (i.e., (1.10)) in the two-contaminant case. Let us discretize the domain  $[0, 1] \times [0, 1]$  by introducing the mesh  $\Omega_{h_{s_1}h_{s_2}} := \{(c_{1,i}, c_{2,j}) : c_{1,i} = ih_{s_1}, c_{2,j} = jh_{s_2}, i = 0, \dots, n_{s_1}, j = 0, \dots, n_{s_2}, n_{s_1} = 1/h_{s_1}, n_{s_2} = 1/h_{s_2}\}$ . In all the experiments in the present section, we consider that  $h_{s_1} = h_{s_2} = h_s$ . We approximate  $Q(c_1, c_2)$  by interpolating it at the mesh nodes with the bilinear spline  $Q_{I,h_s}(c_1, c_2) \in S_1(c_{1,1}, \dots, c_{1,n_{s_1}-1}) \otimes S_1(c_{2,1}, \dots, c_{2,n_{s_2}-1})$ . I.e, we construct the function

$$Q_{I,h_s}(c_1, c_2) = \sum_{i=0}^{n_{s1}} \sum_{j=0}^{n_{s2}} Q(c_{1,i}, c_{2,j}) \phi_i(c_1) \psi_j(c_2), \quad (4.3)$$

where  $\phi(x)$  and  $\psi(x)$  are univariate hat-functions, defined as in (4.2). Plots of two example basis functions,  $\phi_4(c_1)\psi_4(c_2)$ , and  $\phi_5(c_1)\psi_5(c_2)$ , are presented in Figure 4.15. Further information about the bivariate interpolation approach can be found in the Appendix.

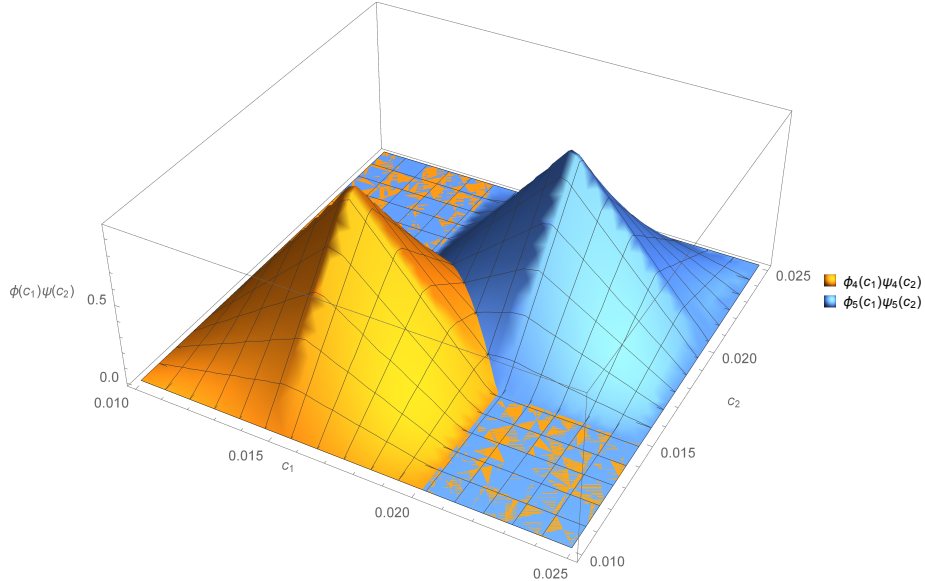


Figure 4.15: Bilinear B-splines.

**Experiment 19.** Bilinear spline interpolation shows very satisfactory results also in the case of two contaminants. The approximations of the load functions  $Q(c_1, c_2)$  for NOM and Furosemide are presented in Figure 4.16. The function and its interpolant seem to be identical on a visual inspection on Figure 4.16. The corresponding results of the numerical solution of the differential problem (1.8), (1.10), (1.11) with the two simultaneous contaminants are depicted in Figures 4.17–4.21.

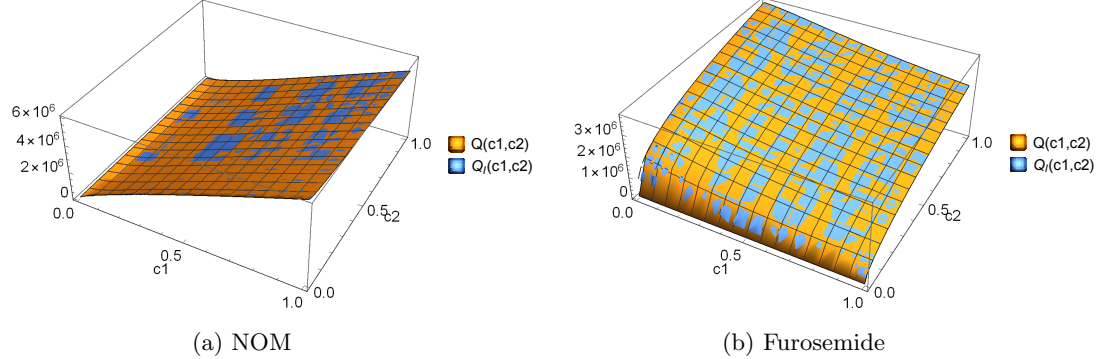


Figure 4.16: **Experiment 19.** Plots of the function  $Q(c_1, c_2)$  and its bilinear interpolant  $Q_{I,h_s}(c_1, c_2)$  for NOM and Furosemide.

The results for NOM, obtained by substitution of the load functions with their interpolants do not differ significantly from those, obtained using the original SIAS model (Figures 4.17 and 4.18). For low concentration values of the micro-pollutant, there are small deviations in the results (Figures 4.19 to 4.21), which is natural, because of the high relative error between the original adsorption capacity of Furosemide and its spline interpolant that we discussed in the univariate case. The qualitative behaviour of the solutions for Furosemide, however, is conserved. Therefore, bilinear spline approximation of the load functions,  $Q_i$ , seems like a reasonable alternative to using the original SIAS definitions if one wants to improve the computational times (as we discuss in the next section).

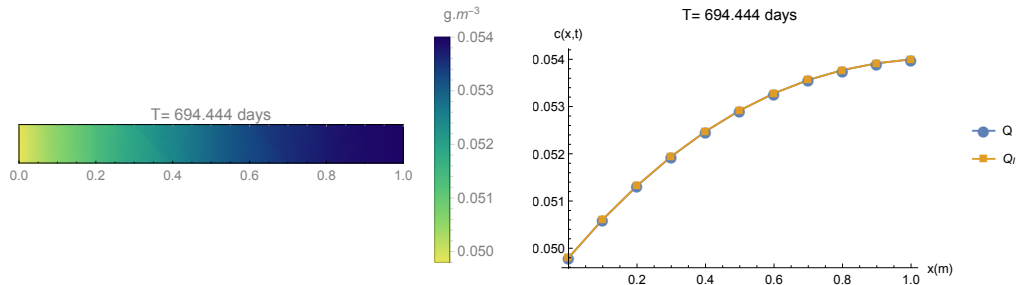


Figure 4.17: **Experiment 19.** Two-component adsorption using bilinear spline interpolation. Results for the concentration  $c$  for NOM.

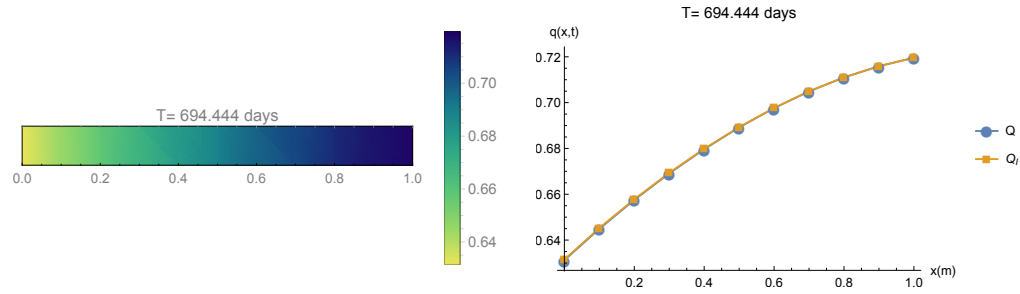


Figure 4.18: **Experiment 19.** Two-component adsorption using bilinear spline interpolation. Results for the load  $q$  for NOM.

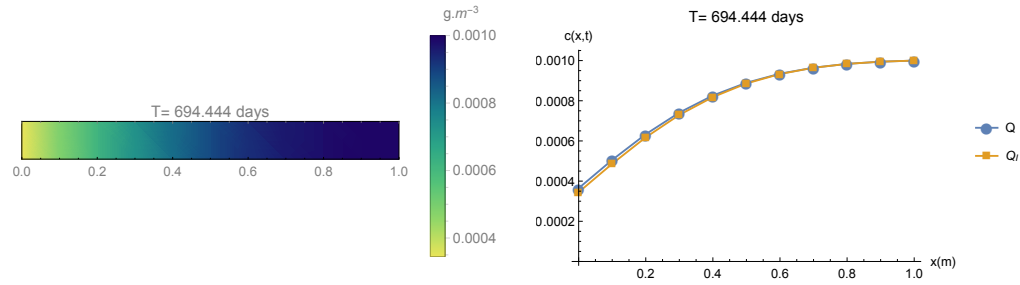


Figure 4.19: **Experiment 19.** Two-component adsorption using bilinear spline interpolation. Results for the concentration  $c$  for Furosemide.

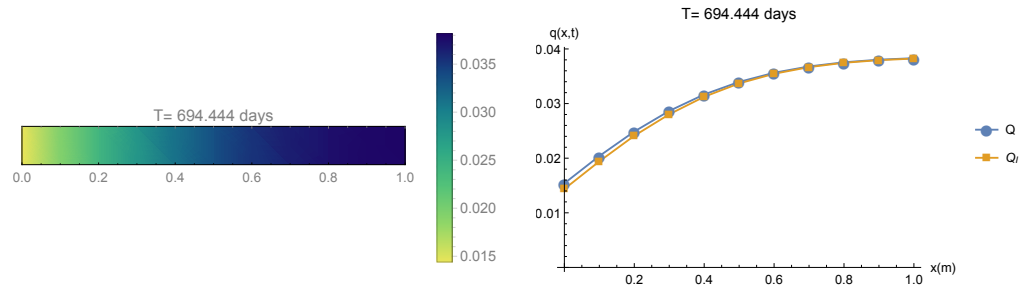


Figure 4.20: **Experiment 19.** Two-component adsorption using bilinear spline interpolation. Results for the load  $q$  for Furosemide.

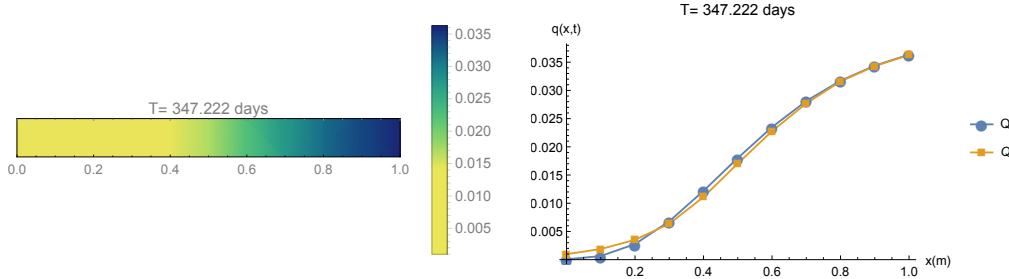


Figure 4.21: **Experiment 19.** Two-component adsorption using bilinear spline interpolation. Results for the load  $q$  for Furosemide.

**Experiment 20.** Let us now compare the computed breakthrough curves of the tested contaminants, when the original load function and its interpolant are used, see Figures 4.22, 4.23. For NOM, the curves are practically identical. For the micro-pollutant, however, a visible difference is observed for lower values of  $c/c_0$ . Nevertheless, the result can be used as a good first approximation from a practical point of view, since filters are changed after a higher threshold is reached. For  $c/c_0 > 0.2$ , the two curves are very close to each other.

If one wants to improve the accuracy, in the two-contaminant case, uniform refinement of the mesh appears to be inapplicable. For example, if the spline step is lowered to  $10^{-6}$ , as in the single contaminant case, the space mesh would contain  $10^{12}$  nodes in which  $Q$  must be evaluated. This operation would take about 2000 hours<sup>1</sup> ! Therefore, we shall consider an adaptive (local) mesh refinement in our future work.

---

<sup>1</sup>as estimated on PC, using the Wolfram Mathematica computer algebra system.

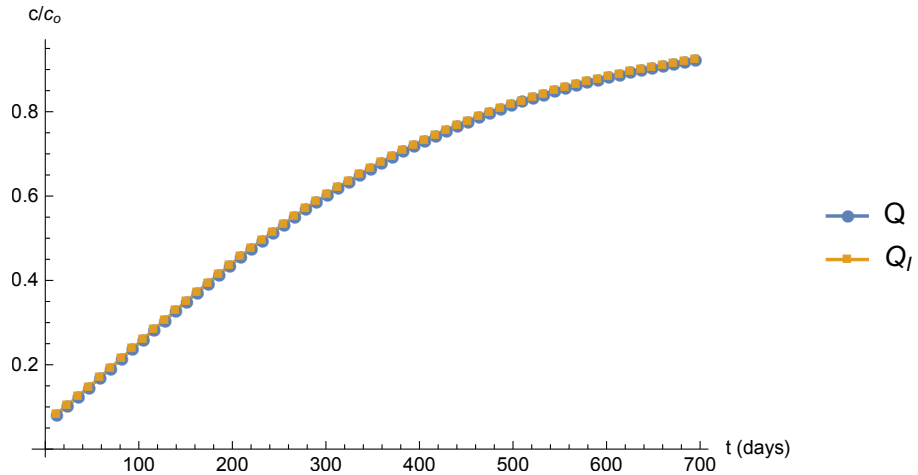


Figure 4.22: **Experiment 20.** Two-component adsorption. Comparison between breakthrough curves for NOM, using  $Q$  and  $Q_I$ .

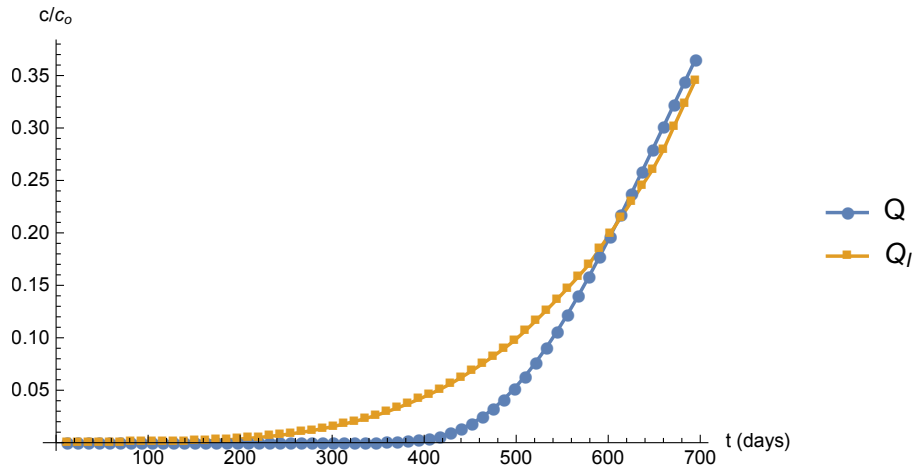


Figure 4.23: **Experiment 20.** Two-component adsorption. Comparison between breakthrough curves for Furosemide, using  $Q$  and  $Q_I$ .

### Computational times

The primary purpose of interpolating the load functions was that the SIAS model has big time complexity, as commented in Section 2.3. The numerical experiments, presented above, showed that the approximation of the load function with linear/bilinear splines is applicable, on the one hand, because it

describes very well the original behaviour of the function  $Q$ , and, on the other hand, because it allows the computations to be made much quicker. First of all, the evaluation of the function  $Q$ , defined as in (1.10) at a point is significantly slower than the evaluation of the respective interpolant, as shown in Table 4.1. This fact, naturally, leads to quicker solution of the mathematical model. In Table 4.2 the time in seconds, needed for solving the mathematical model, using the piecewise-linear approximation for the load function is presented. The timing results, obtained using the original definition, are presented again for comparison. As one can see, the CPU time needed for solving the model using the bilinear interpolant in the two-contaminant case, is significantly lower than the time needed for solving the model, using the definition (1.10). If generalized successfully to the multi-component case, this approach would probably give a very distinct reduction of the computational time, needed for the model solving. Such generalization, however, is not included in the Master's thesis but is one of the important topics on which we shall focus in our future work.

Number of contaminants	SIAS	Interpolant
1	4.21203	0.171601
2	6.75484	0.187201

Table 4.1: CPU time in seconds needed for evaluating the load function  $10^6$  times with its original definition (1.10) and its linear/bilinear interpolant.

Number of contaminants	SIAS	Interpolant
1	10.7641	6.16204
2	384.667	280.505

Table 4.2: CPU time in seconds needed for solving the model (1.8), (1.10), (1.11), using the linear/bilinear approximation of the load function.

# Conclusions and perspectives

Water purification is an important contemporary subject, with which a lot of commercial and non-commercial organizations are concerned. Mathematical modelling of this process appears to be a powerful tool for investigation of its qualitative and quantitative behaviour, which, in turn, helps the industry on the one hand to improve its quality, and, on the other hand, to reduce operational costs. The KWR Watercycle Research Institute, in particular, aims to provide solutions for treatment of surface water, which comprises around 40% of the drinking water in the Netherlands [12]. They met some difficulties, concerning the numerical solution, related to the convergence of the numerical schemes they have used for specific parameter values.

In the Master's thesis, a robust numerical scheme was constructed. It is based on a fully-implicit approximation of the first equation of (1.8) and an explicit approximation of the second equation. Its applicability is verified by conducting various experiments with values of the model parameters that would be encountered in practice. The time evolution of the concentration and load of up to 10 different contaminants as well as the corresponding breakthrough curves were computed successfully. Another semi-implicit approximation, which is more computationally effective, is shown to be applicable for values of  $\gamma$  greater than  $10^{-5}$ . A practical estimate for the rate of convergence shows that the fully-implicit scheme has first order of convergence. As a future work, we shall consider the construction of higher order schemes.

Furthermore, in order to make the numerical algorithm more computationally effective, spline-based approximation of the load function, which gives promising results, was suggested in the cases of one and two contaminants. In order to fully implement this idea, we shall try to generalize it in the multiple-contaminant case. Formally speaking, the generalization of (4.3) is trivial. However, to use it in practice, one needs to construct an appropriate mesh generation algorithm for the interpolation nodes.

As a further development of the present study, we shall undertake the following steps. We shall compare the quantitative results to experimental data. Such data has been recently provided to us by KWR. An example breakthrough curve is depicted below (Figure 4.24).

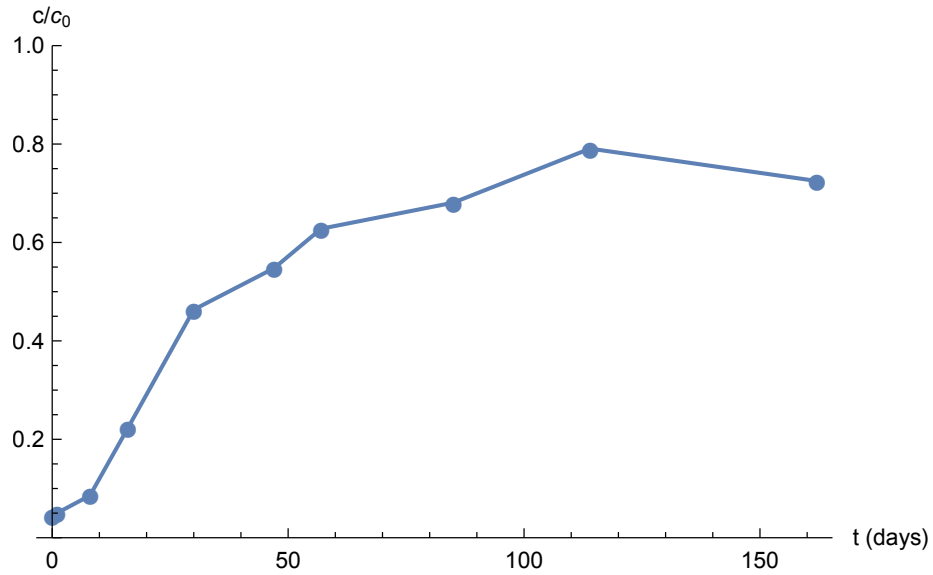


Figure 4.24: Breakthrough curve for the micro-pollutant Urotropine, provided by KWR.

Also, the model can be generalized by introducing terms describing the bioreactivity in the filter (i.e., the formation of a biofilm on the carbon particles), following [1]. Further generalizations in 2D or 3D can be considered that incorporate the simulation of the water flow inside the porous medium. The numerical methods should be developed and extended correspondingly.

# Bibliography

- [1] L.T.J. van der Aa, L.C. Rietveld, J.C. van Dijk, Simultaneous removal of natural organic matter and atrazine in biological granular activated carbon filters: model validation, IWA Specialist Conference ‘Water and Wastewater Treatment Plants in Towns and Communities of the XXI Century: Technologies, Design and Operation’, Moscow, Russia. 2010.
- [2] B. Boyanov, Lectures in Numerical Methods (in Bulgarian), Darba, 2008.
- [3] F. Cecen, O. Aktas, Activated Carbon for Water and Wastewater Treatment. Integration of Adsorption and Biological Treatment, WILEY-VCH Verlag GmbH & Co. KGaA, 2011.
- [4] Z.Z. Chowdhury, S.B. Abd Hamid, S.M. Zain, Evaluating design parameters for breakthrough curve analysis and kinetics of fixed Bed Columns for Cu(II) Cations Using Lignocellulosic Wastes, BioRes. 10 (2015) 732–749.  
<https://doi.org/10.15376/biores.10.1.732-749>
- [5] F.A. DiGiano, G. Baldauf, B. Frick, H. Sontheimer, Simplifying the description of competitive adsorption for practical application in water treatment, Activated Carbon Adsorption of Organics from the Aqueous Phase 1 (1980) 213–228.
- [6] S. Dimova, T. Chernogorova, A. Yotova, Numerical methods for Differential Equations (in Bulgarian), Sofia University Publishing house, 2010.
- [7] H. Freundlich, Kapillarchemie, eine Darstellung der Chemie der Kolloide und verwandter Gebiete, Akademische Verlagsgesellschaft, 1909.  
<https://doi.org/10.1038/085534a0>
- [8] P. Harris, Z. Liu, K. Suenaga, Imaging the atomic structure of activated carbon, Journal of Physics: Condensed Matter 20 (2008) 362201.  
<https://doi.org/10.1088/0953-8984/20/36/362201>
- [9] D. Hendricks, Fundamentals of Water Treatment Unit Processes. Physical, Chemical, and Biological, CRC Press, 2011.
- [10] V. Inglezakis, S. Poulopoulos, Adsorption, Ion Exchange and Catalysis. Design of Operations and Environmental Applications, Elsevier Science, 2006.

- [11] A.L. Myers, J.M. Prausnitz, Thermodynamics of mixed-gas adsorption, AIChE Journal 11 (1965) 121—127.  
<https://doi.org/10.1002/aic.690110125>
- [12] Proceedings of the 148<sup>th</sup> European Study Group ISBN:978-94-6395-192-0.
- [13] M.Suzuki, Adsorption Engineering, Elsevier, 1990.
- [14] D.R. Younge, T.M. Keinath, The effects of non-ideal competition on multi-component adsorption equilibria, Water Pollut. Control Fed. 58 (1986) 77–81.  
[https://doi.org/10.1016/0043-1354\(91\)90021-H](https://doi.org/10.1016/0043-1354(91)90021-H)

**Online resources (up-to-date as of 09 March, 2020):**

- [15] Activated carbon basics  
<https://www.haycarb.com/activated-carbon>
- [16] Activated carbon filters  
<https://condorchem.com/en/activated-carbon-filters/>
- [17] Carbamazepine, Wikipedia  
<https://en.wikipedia.org/wiki/Carbamazepine>
- [18] Cortisol, Wikipedia  
<https://en.wikipedia.org/wiki/Cortisol>
- [19] Desorption, Wikipedia  
<https://en.wikipedia.org/wiki/Desorption>
- [20] Development of PHREEQC database for Surface complexation modelling of Arsenic on Nano magnetite  
[https://www.ndsu.edu/pubweb/\\_sainieid/geochem/talks/Das-Surface-Complexation-Modelling-Arsenic-Nano-Magnetite.pdf](https://www.ndsu.edu/pubweb/_sainieid/geochem/talks/Das-Surface-Complexation-Modelling-Arsenic-Nano-Magnetite.pdf)
- [21] Diclofenac, Wikipedia  
<https://en.wikipedia.org/wiki/Diclofenac>
- [22] Quiz: Write one similarity between Physisorption and Chemisorption  
<https://goprep.co/write-one-similarity-between-physisorption-and-chemisorption-i-1nk8fj>
- [23] Organic matter, Wikipedia  
[https://en.wikipedia.org/wiki/Organic\\_matter](https://en.wikipedia.org/wiki/Organic_matter)
- [24] Furosemide, Wikipedia  
<https://en.wikipedia.org/wiki/Furosemide>
- [25] Information, provided by KWR in personal communication

- [26] Intermolecular forces, structure and properties  
<http://www.chemhume.co.uk/ASCHEM/Unit%201/Ch3IMF/Chemical%20Struct.htm>
- [27] Ketoprofen, Wikipedia  
<https://en.wikipedia.org/wiki/Ketoprofen>
- [28] KWR Water Research Institute Website  
<https://www.krwater.nl/en/>
- [29] Pentoxifylline, Wikipedia  
<https://en.wikipedia.org/wiki/Pentoxifylline>
- [30] Phenazone, Wikipedia  
<https://en.wikipedia.org/wiki/Phenazone>
- [31] Sulfachloropyridazine  
<https://pubchem.ncbi.nlm.nih.gov/compound/sulfachloropyridazine>
- [32] Tensor Product Spline Surfaces, INF-MAT5340—Spline methods—University of Oslo—Teaching materials  
<https://www.uio.no/studier/emner/matnat/ifi/nedlagte-emner/INF-MAT5340/v07/undervisningsmateriale/kap7.pdf>
- [33] Trimethoprim, Wikipedia  
<https://en.wikipedia.org/wiki/Trimethoprim>

# Appendix A

## Breakthrough curves

As mentioned in Section 1.2, when studying the process of adsorption, the experiments are made in a stirred batch reactor without source and outlet. In this experimental environment, the total amount of the polluted solution and adsorbent material do not change during the whole process. The adsorption process continues until an equilibrium is reached between the concentrations of adsorbate in the solid and the liquid phases. However, in a fixed-bed column, there is a continuous flow of the polluted liquid in and out of the carbon bed filter, whereas the amount of the adsorbent stays unchanged. Therefore, inside an adsorber the concentrations of contaminants change with respect to both time and reactor length. This concentration dynamics can be described using the ratio  $c/c_0$ , where  $c$  is the effluent (outlet) concentration of contaminant and  $c_0$  is the influent concentration, expressed as functions of elapsed time. The plot of this ratio is termed “the breakthrough curve”. Figure A.2 shows different moments of the adsorption process (on the top), and the corresponding breakthrough curve (at the bottom).

The flow of polluted water creates a so-called wave front through the adsorbent bed (the wave front usually refers to “the region of rapid change in concentration”). The part of the wave front, covering the area near the inlet in the beginning of the process, is known as mass transfer zone (MTZ) (Figure A.2). This is the zone in which the actual adsorption takes place. With the exhaustion of the activated carbon with time, MTZ moves downwards through the bed. When MTZ travels forward, it leaves behind a portion of the carbon that is saturated by the contaminants. The breakthrough curve can also be regarded as the graphical representation of MTZ movement through the carbon column. Theoretically, when MTZ reaches the bottom of the column, breakthrough occurs. However, in practice, the breakthrough point is detected, when the value of the ratio between influent and outlet concentrations ( $c/c_0$ ) reaches a specific predetermined value, which is usually selected according to purity requirements. The breakthrough threshold can take a large variety of values—in the range [0.05, 0.9] as shown in Figure A.1.

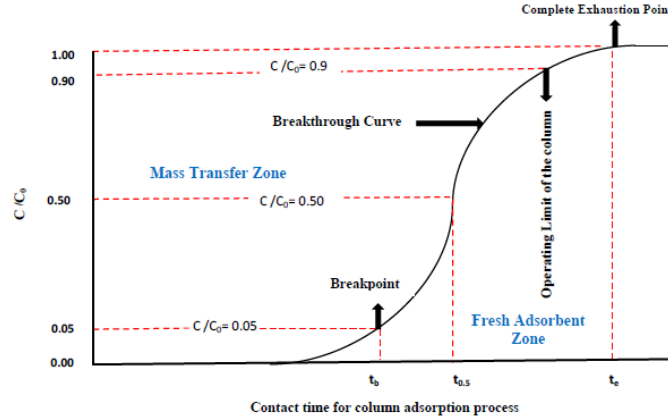


Figure A.1: Breakthrough curve characteristics in a fixed-bed with respect to time.

A filter is usually replaced/regenerated at the value of 0.5 for  $c/c_0$ . The column adsorption capacity is often calculated at this point. The column can still operate after this point, until  $c/c_0$  reaches a value of about 0.9. This point is termed the operating limit of the column. The column will be completely exhausted when the inlet concentration becomes almost equal to the outlet one, i.e.,  $C_0 = C$  (Figure A.1).

The bed height, the inlet concentration and the flow rate are some of the factors, influencing the shape of the breakthrough curve. In presence of bioactivity in the reactor, the shape of the curve can be altered significantly [4].

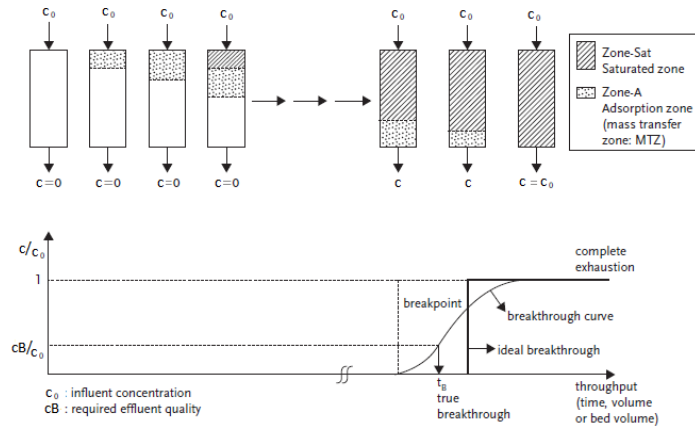


Figure A.2: Breakthrough characteristics in a GAC adsorber [3].

# Appendix B

## Management of spent material

The adsorptive capacity of carbon filters is gradually decreased with time and finally exhausted. The exhausted carbon is also termed as “spent” and has to be treated in an appropriate manner in order to be reused. The possibilities for treatment of spent carbon are regeneration, reactivation or eventual disposal. Treatment of water and wastewater with activated carbon involves a large capital investment and very high operating costs. The regeneration/reactivation of spent adsorbents is the most difficult and expensive part of the adsorption technology. It accounts for about 75% of total operating and maintenance cost for a fixed-bed GAC operation [3].

Although the terms regeneration and reactivation are usually used interchangeably, regeneration means removal of the contaminants without destroying them, whereas reactivation means that the carbon filter is put under an activation process, running at a very high temperature, which leads to the destruction of the adsorbed contaminants.

There exist cases in which the regeneration/reactivation of spent carbon is either technically or economically not viable. For example, the carbon can be irreversibly contaminated by the adsorbed substance, or the regeneration process may be too costly, mainly when the adsorbed species are dangerous (e.g., toxic or radioactive substances). For example, if a PAC reactor was used for the removal of heavy metals, the disposal of the spent material is the most appropriate method [10].

During the process of regeneration neither the carbon, nor the contaminants are destroyed. Regeneration is usually accomplished with the means of pressure and temperature, where the contaminants are being volatilized. The contaminants are recovered as a liquid after a condensation step. Therefore, the regeneration process should be accompanied by a proper waste treatment mechanism, because the desorbed contaminants produce a waste stream.

The process of reactivation of carbon is conducted at a very high temperature

(typically in excess of 800°C). This temperature is able to destruct not only the adsorbed substances, but the carbon filter itself. Carbon losses due to reactivation can be held at 3–15 % [10].

## Appendix C

# Spline interpolation basics

Here, we outline some of the basics of spline interpolation theory that are used in the thesis [2, 32].

### C.1 Univariate spline interpolation

Spline interpolation is a form of interpolation in which the interpolating function is a piecewise polynomial function with additional smoothness requirements. It is often preferred over polynomial interpolation because of the fact that a relatively high accuracy can be achieved, even when using low degree splines.

**Definition 1.** [2] The function  $s(x)$  is called a spline-function of degree  $r$  with knots  $x_1 < \dots < x_n$ , if:

1.  $s(x)$  is a polynomial of degree at most  $r$  over each interval  $(x_i, x_{i+1})$ ,  $i = 0, \dots, n$ , ( $x_0 = -\infty, x_{n+1} = \infty$ );
2.  $s(x), s'(x), \dots, s^{(r-1)}(x)$  are continuous functions in  $(-\infty, \infty)$ .

The set of all spline functions of order  $r$  with knots  $x_1, \dots, x_n$  is commonly denoted with  $S_r(x_1, \dots, x_n)$ . In particular, B-spline or basis spline is a spline function that has minimal support with respect to a given degree, smoothness, and domain partition. The latter is formalized in Theorem 1 below.

**Definition 2.** [2] The divided difference of the truncated power function  $(\bar{x} - x)_+^{r-1}$  with respect to  $\bar{x}$  at the points  $x_0 < \dots < x_r$  is called B-spline of degree  $r-1$  with knots  $x_0, \dots, x_r$ . We shall denote it by  $B(x_0, \dots, x_r; x)$ .

Let us note that  $B(x_0, \dots, x_r; x) \in S_{r-1}(x_0, \dots, x_r)$  [2].

**Theorem 1.** [2] For each  $r \geq 1$ , the following holds true:

$$\begin{aligned} B(x_0, \dots, x_r; x) &= 0 \text{ for each } x \leq x_0 \text{ and for each } x \geq x_r, \\ B(x_0, \dots, x_r; x) &> 0, \text{ for } x \in (x_0, x_r). \end{aligned}$$

The proof can be found in [2].

The main result, related to B-splines application is stated by the following Theorem:

**Theorem 2.** [2] Let  $a < x_{r+1} < \dots < x_n < b$  are fixed points and let us choose another  $2r$  arbitrary points  $x_1 < \dots < x_r < a$  and  $b < x_{n+1} < \dots < x_{n+r}$ . Let  $B_i(x) := B(x_i, \dots, x_{i+r}; x)$ ,  $i = 1, \dots, n$ . Then the B-splines  $B_1, \dots, B_n$  form a basis of the space  $S_{r-1}(x_{r+1}, \dots, x_n)$  over the interval  $[a, b]$ .

The proof can be found in [2].

So, each spline-function  $s \in S_{r-1}(x_{r+1}, \dots, x_n)$ , has a unique representation in the form

$$s(x) = \sum_{i=1}^n \alpha_i B_i(x) \quad (\text{C.1})$$

in the interval  $x \in [a, b]$ . For all the numerical results, presented in the thesis, first-order splines (i.e., piecewise-linear polynomials) are used. Normalizing the linear B-splines, one can introduce the interpolation basis of the space of piecewise-linear functions  $S_1(x_1, \dots, x_{n-1})$ , depicted in Figure C.1. The basis functions are defined as follows:

$$\begin{aligned} \phi_0(x) &= \begin{cases} \frac{x_1 - x}{x_1 - x_0}, & x \in [x_0, x_1], \\ 0, & x > x_1, \end{cases} \\ \phi_i(x) &= \begin{cases} \frac{x - x_{i-1}}{x_i - x_{i-1}}, & x \in [x_{i-1}, x_i], \\ \frac{x_{i+1} - x}{x_{i+1} - x_i}, & x \in [x_i, x_{i+1}], \\ 0, & \text{otherwise,} \end{cases}, \quad i = 1, \dots, n-1, \quad (\text{C.2}) \\ \phi_n(x) &= \begin{cases} \frac{x - x_{n-1}}{x_n - x_{n-1}}, & x \in [x_{n-1}, x_n], \\ 0, & x < x_{n-1}. \end{cases} \end{aligned}$$

Taking into account the latter, and also the fact that the functions, defined with (C.2) form an interpolation basis (Figure C.1), the coefficients  $\alpha_i, i = 1, \dots, n$  in the linear combination (C.1), are  $\alpha_i = s(x_i)$ .

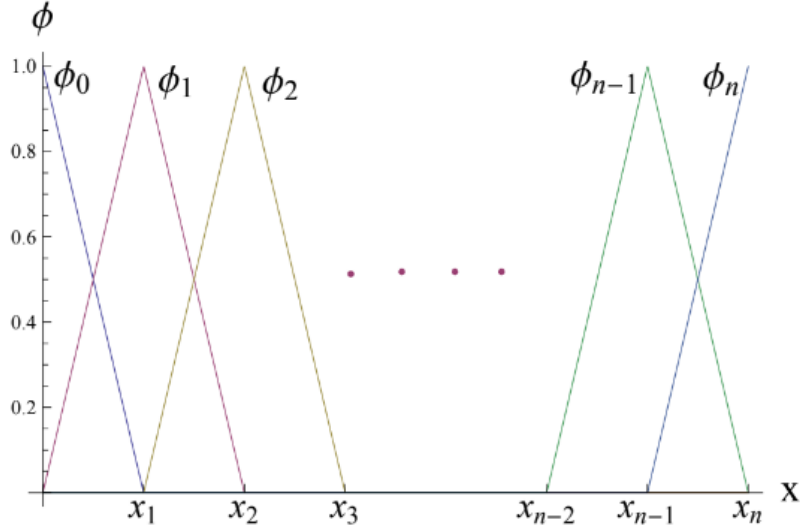


Figure C.1: Nodal basis of the space of piecewise linear functions.

## C.2 Bivariate spline interpolation

In the two-contaminant case, the spline interpolation needs to be generalized in two dimensions. We shall discuss one possible approach to construct surfaces using univariate functions, following [32].

Let us introduce the idea on the basis of bilinear polynomials. If we want to construct a line segment with endpoints  $a_0$  and  $a_1$  for  $x \in [0, 1]$ , we can take:

$$a_0(1 - x) + a_1 x.$$

Let us now suppose that  $a_0 = a_0(y)$  and  $a_1 = a_1(y)$  are two functions, defined for  $y \in [c, d]$ . Then, for each  $y \in [c, d]$  the function  $a_0(y)(1 - x) + a_1(y)x$  is a line segment connecting  $a_0(y)$  and  $a_1(y)$ , and when  $y$  varies we will get a family of straight lines representing the surface:

$$z = a_0(y)(1 - x) + a_1(y)x,$$

where  $a_0(y)$  and  $a_1(y)$  can be arbitrary functions. If we consider the special case, taking  $a_0(y)$  and  $a_1(y)$  to be linear polynomials, specifically

$$a_0(y) = b_{0,0}(1 - y) + b_{0,1}y, \quad \text{and} \quad a_1(y) = b_{1,0}(1 - y) + b_{1,1}y,$$

we shall obtain a bilinear polynomial

$$f(x, y) = b_{0,0}(1 - x)(1 - y) + b_{0,1}(1 - x)y + b_{1,0}x(1 - y) + b_{1,1}xy. \quad (\text{C.3})$$

In fact, the coefficients are the values of  $f$  at the corners of the unit square  $(x, y) \in [0, 1] \times [0, 1]$ .

We can construct spline surfaces from families of spline functions, using a similar idea. Using the notation from Section C.1, suppose that for some knot vector  $(x_0, \dots, x_n)$ , we have constructed the spline space

$$S_x = S(x_1, \dots, x_{n1-1}) = \text{span}\{\phi_0, \dots, \phi_{n1}\},$$

where  $\{\phi_i\}_{i=0}^{n1}$  are functions in  $x$ , defined with (C.2), corresponding to the given knot vector. Let us now take a linear combination of those functions with coefficients  $c_i$  that are functions of  $y$ :

$$f(x, y) = \sum_{i=0}^{n1} c_i(y) \phi_i(x). \quad (\text{C.4})$$

Thus, for each fixed value of  $y$ ,  $f(x, y) \in S_x$ , and when  $y$  varies, we obtain a family of spline functions, each depending on  $x$ . Now, suppose that we have another set of knots  $(y_0, \dots, y_{n2})$ . Then, we can construct another spline space

$$S_y = S(y_1, \dots, y_{n2-1}) = \text{span}\{\psi_0, \dots, \psi_{n2}\},$$

where  $\{\psi_i\}_{i=0}^{n2}$  denote the basis analogous to (C.2) in  $S_y$ . Then, if each coefficient  $c_i(y)$  in (C.4) is from  $S_y$ ,

$$c_i(y) = \sum_{j=0}^{n2} c_{i,j} \psi_j(y), \quad (\text{C.5})$$

for suitable coefficients  $\{c_{i,j}\}_{i,j=0}^{n1,n2}$ .

Combining (C.4) and (C.5), we obtain the bilinear spline

$$f(x, y) = \sum_{i=0}^{n1} \sum_{j=0}^{n2} c_{i,j} \phi_i(x) \psi_j(y). \quad (\text{C.6})$$

The functions  $\{\phi_i(x) \psi_j(y)\}_{i,j=1}^{n1,n2}$  form an interpolation basis of the space of bilinear splines in  $(x, y) \in [0, 1] \times [0, 1]$ . They have the shape of a curved pyramid with value one at the top (see Figure C.2).

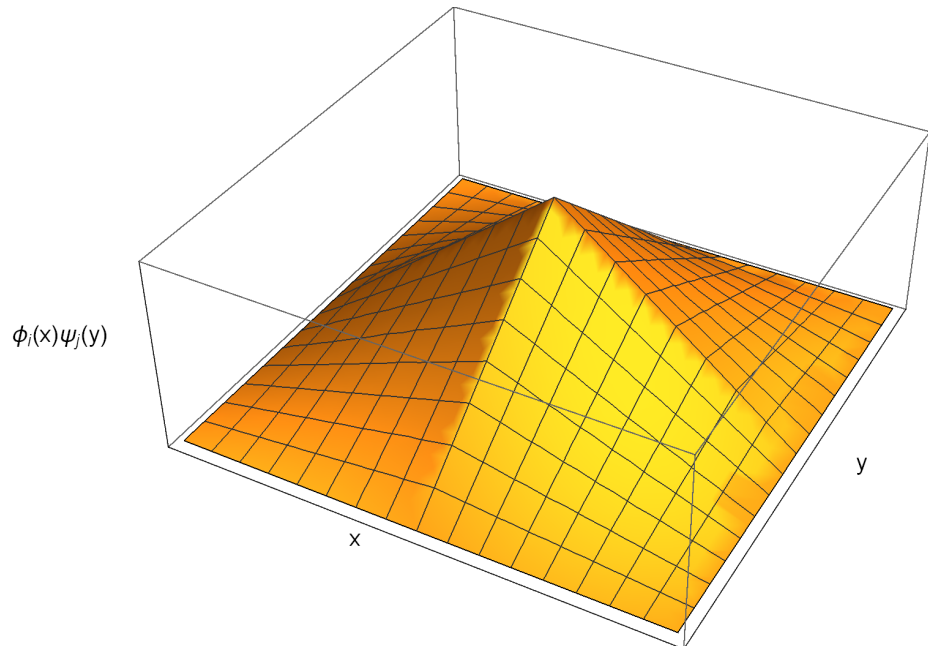


Figure C.2: Bilinear B-spline.

There are a lot of ways to construct surfaces from two spaces of univariate functions, but the one, presented above, has one great advantage: we can easily obtain generalizations of many univariate operations when we need to perform them on such surfaces. One of the most important features of this approach is its computational efficiency. As shown in [32], the computation of the value  $f(x, y)$  can be done with only 16 multiplications. Furthermore, the approach is easily generalizable to higher order spline surfaces and more dimensions.